NASA CR-135102

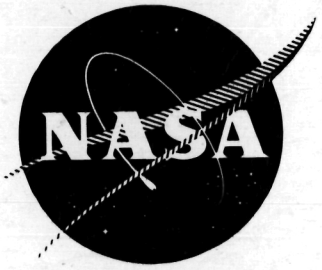

ARGON HOLLOW CATHODE

PREPARED FOR

LEWIS RESEARCH CENTER

NATIONAL AERONAUTICS AND SPACE ADMINISTRATION

GRANT NSG-3011

by

Larry A. Rehn

Approved by

Harold R. Kaufman

November 1976

Department of Mechanical Engineering
Colorado State University
Fort Collins, Colorado

1 Report No	2 Government Accession No	3 Recipient's Catalog No
NASA CR-135102		

4 Title and Subtitle	5 Report Date
ARGON HOLLOW CATHODE	November 1976
	6 Performing Organization Code

7 Author(s)	8 Performing Organization Report No
Larry A. Rehn	
	10 Work Unit No

9 Performing Organization Name and Address	11 Contract or Grant No
Department of Mechanical Engineering Colorado State University Fort Collins, Colorado 80523	NSG-3011
	13 Type of Report and Period Covered
12 Sponsoring Agency Name and Address	Contractor Report
National Aeronautics and Space Administration Washington, D.C. 20546	14 Sponsoring Agency Code

15 Supplementary Notes
Grant Manager - Michael J. Mirtich, Jr.
NASA Lewis Research Center, Cleveland, Ohio 44135
This report is a reproduction of the M.S. Thesis of Mr. Larry A. Rehn.

16 Abstract

An interest in alternate propellants for ion-bombardment thrusters, together with ground applications of this technology, has prompted consideration of argon. Several variations of conventional hollow cathode designs were tried, but the bulk of the testing used a hollow tube with an internal tungsten emitter and an orifice at one end. The optimum cathode tube diameter was found to be in the range of 1.0-2.5 cm, somewhat larger than those used for cesium and mercury Optimum orifice diameter depended on operating conditions, and varied from 0.5 to 5 mm. Biasing the internal emitter negative relative to the cathode chamber reduced the external coupling voltage and should therefore improve orifice lifetime. The expected effect of this bias on emitter lifetime was less clear. Lifetime tests were not conducted as part of this investigation, but several designs show promise of long lifetime in specific applications.

17 Key Words (Suggested by Author(s))	18 Distribution Statement
Hollow cathodes Electron emission Ion sources	Unclassified - unlimited

19 Security Classif (of this report)	20 Security Classif (of this page)	21 No of Pages	22 Price*
Unclassified	Unclassified		

* For sale by the National Technical Information Service Springfield Virginia 22161

NASA-C-168 (Rev 10-75)

TABLE OF CONTENTS

I. INTRODUCTION

The use of cesium and mercury as propellant for hollow cathodes and electron-bombardment ion thrusters has been successfully demonstrated for space missions.[1] These elements exhibit at least three advantages over other potential propellants; ease of storage, ease of ionization, and high atomic weight. The latter tends to reduce discharge power loss relative to the kinetic energy of the beam ion. Argon and xenon gases have also been studied,[2-5] first from a research viewpoint, and later as alternate propellants for space propulsion because of their environmental advantages. Of the two gases, xenon is preferable in all respects for space propulsion except for cost and availability. Argon becomes cost effective as a space propellant if used in sufficient quantities as to make cryogenic storage practical.[6]

A major problem with argon has been the rapid wear that results when it is used in hollow cathodes. Hollow cathodes with lifetimes of 10,000 hours or more when used with mercury,[1,5-7] have been found to be the only cathodes suitable for ion thrusters for space missions. The main objective of this study was the development of a similar long life hollow cathode for argon. A secondary objective was ease and reliability of starting. Argon was emphasized in this study both because it is of interest as a propellant and because it is a greater departure than xenon from the usual thruster propellants of cesium and mercury.

A thermionic emitter of tungsten located inside a conventional hollow cathode tube was selected for this study. Hopefully, a thermionic emitter could have a longer lifetime inside a hollow cathode than exposed to the ion-chamber discharge. If so, the internal emitter would also facilitate starting without the use of high voltage. Another

important reason for the selection of an internal emitter, though, was to obtain reproducible emission characteristics without the coating and conditioning problems of the oxide impregnated inserts used in conventional hollow cathodes. These inserts generally contain barium-strontium oxides which aid electron emission by reducing the work function of the cathode interior surface.[9, 10] Fig. 1 contrasts a conventional hollow cathode with a typical design used herein.

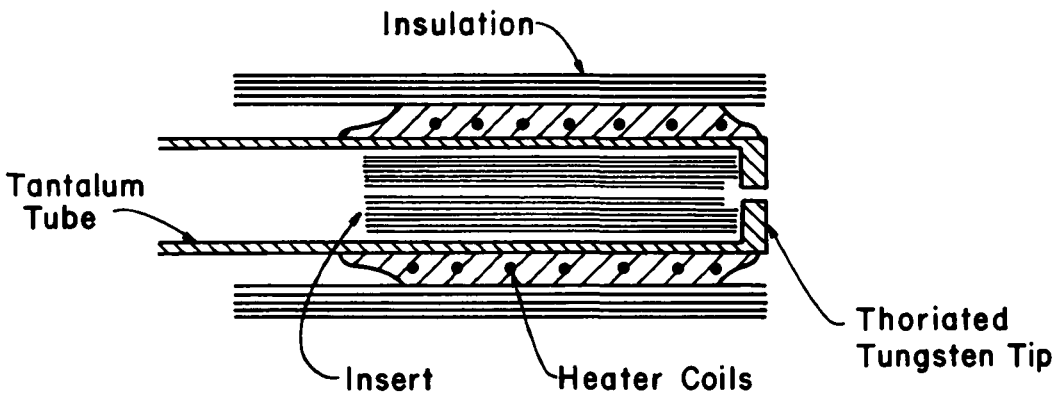

(a.) Conventional Hollow Cathode

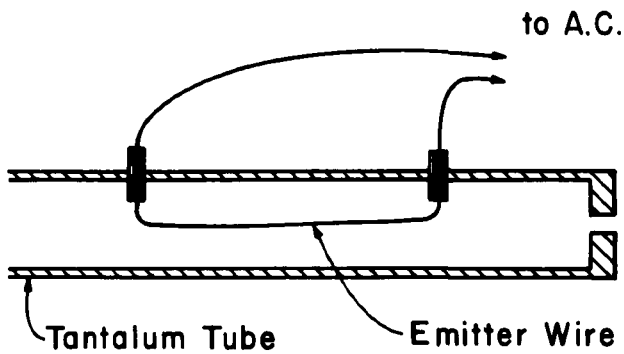

(b) 0.64 cm Cathode with Internal Emitter

Figure 1. Comparison of conventional hollow cathode with the proposed design.

II. CATHODE LIFETIME

Cathode lifetimes of $\geq$ 10,000 hours are a requirement for practical use in space.[7] A simple refractory-metal emitter is a logical choice for a cathode, but ion-bombardment limit their lifetimes to roughly 1000 hours or less.[11] Several other types of cathodes have been tried, but all have some shortcomings. The best choice for space thrusters has been a hollow cathode with an oxide impregnated insert as shown in Fig. 1(a).[7,9] When run on mercury, hollow cathodes attain the desired lifetime of 10,000 hours, but, with argon, rapid erosion reduces the lifetime to only 10-100 hours.[12]

An explanation that has been considered for this lifetime discrepancy is that mercury or cesium vapor is adsorbed on the surface of the cathode which protects it from ion bombardment. Adsorption data for mercury indicates that such a monolayer does not exist for pressures below about 10^{-4} torr or for temperatures much above 300°C.[13] These boundary values are fairly constant for different ion energies. The tip of a hollow cathode is around 1000°C and pressure inside is roughly 1-20 torr.[14] Therefore, monolayer adsorption of mercury may be possible for the pressures in the hollow cathode, but it appears that the temperature would be too high.

In the case of argon the chance for cathode protection due to adsorption is virtually nonexistent. To obtain a monolayer of adsorbed argon, pressures must be above 1 torr and the temperature of the surface must be below 80°K (-193°C).[15] Clearly, cathode protection due to propellant adsorption is not possible for argon and unlikely for mercury.

For conventional hollow cathodes sputtering erosion of the orifice is the major cause of cathode failure. To obtain the desired lifetimes requires that the bombarding ions have energies no greater than 10-20 eV. This energy is determined in the configuration used by the discharge voltage, which couples the cathode and anode. The primary effort of the investigation was to attempt to reduce discharge voltage to 10-20 volts, thereby decreasing orifice wear. Incorporation of a hollow cathode into an actual thruster will, of course, require isolation of the cathode from the discharge, such as accomplished by the baffle and pole piece arrangement in SERT II.[1] This isolation was not a part of the investigation described herein.

III. APPARATUS AND PROCEDURE

All testing was done at the Engineering Research Center of Colorado State University. Initial tests were conducted in a 30 cm bell jar facility, while later tests used one with a 45 cm bell jar. Although both facilities employed 15-cm diffusion pumps, the larger facility gave nearly a factor of ten lower pressure. The major components of the electrical system are indicated in Fig. 2. The thruster simulator was a complete 15-cm axial field thruster, except that no accelerator grid or neutralizer were included. The thruster simulator provided a good model of an actual thruster discharge chamber without the employment of high-voltage supplies. When the apparatus was used to simulate a thruster the magnet current (I_m) was 2 amperes; sufficient to keep primary electrons from directly reaching the anode. Higher field strengths gave no significant difference in cathode performance. Calculations indicated that screen grid blockage should result in a discharge-chamber pressure of 1.55-2.0 times the ambient bell jar pressure for a flow rate of 1000-500 ma-equivalent of argon. The calculation procedure used is shown in the Appendix. The bell jar pressures, when given, are therefore indicative of discharge-chamber pressure. (Also, note that the pressures in all figures are indicated pressures, and must be reduced by a factor of 1.1 for argon and 2.5 for xenon.)

The cathode assemblies were all cylindrical, but otherwise varied widely in configuration. Except for the magnetic orifice and discharge chamber cathodes, they were functionally similar to the version shown attached to the thruster simulator in Fig. 3. Diameters (d) varied from 0.64 cm to 7.6 cm, while lengths (l) were normally maintained at

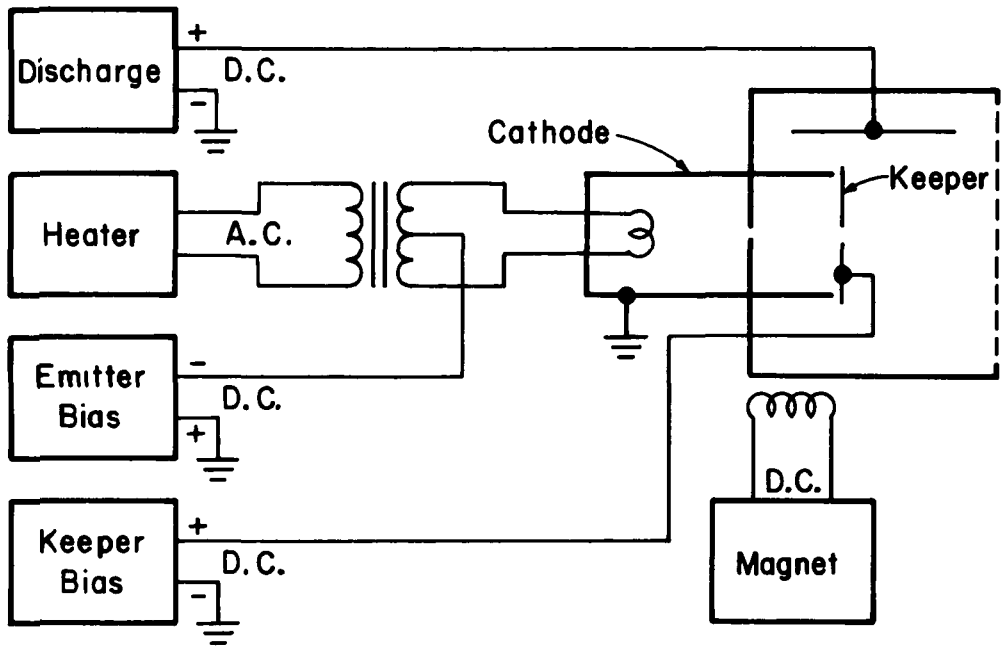

(a) All Cathodes Except Discharge-Chamber Cathode.

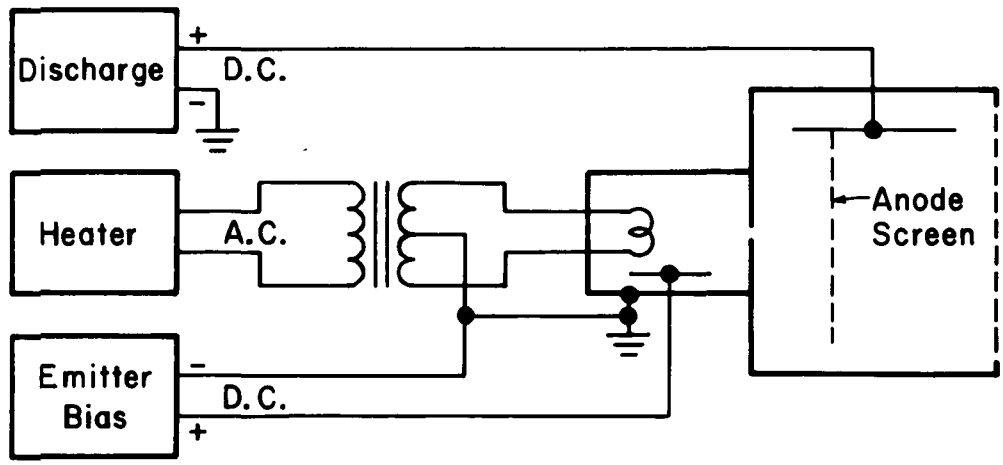

(b) Discharge-Chamber Cathode.

Figure 2. Power supply block diagram. The use of the enclosed keeper, screen anode, and discharge chamber magnet were optional. The screen anode was used with the other cathodes, but always with the discharge chamber electromagnet turned off.

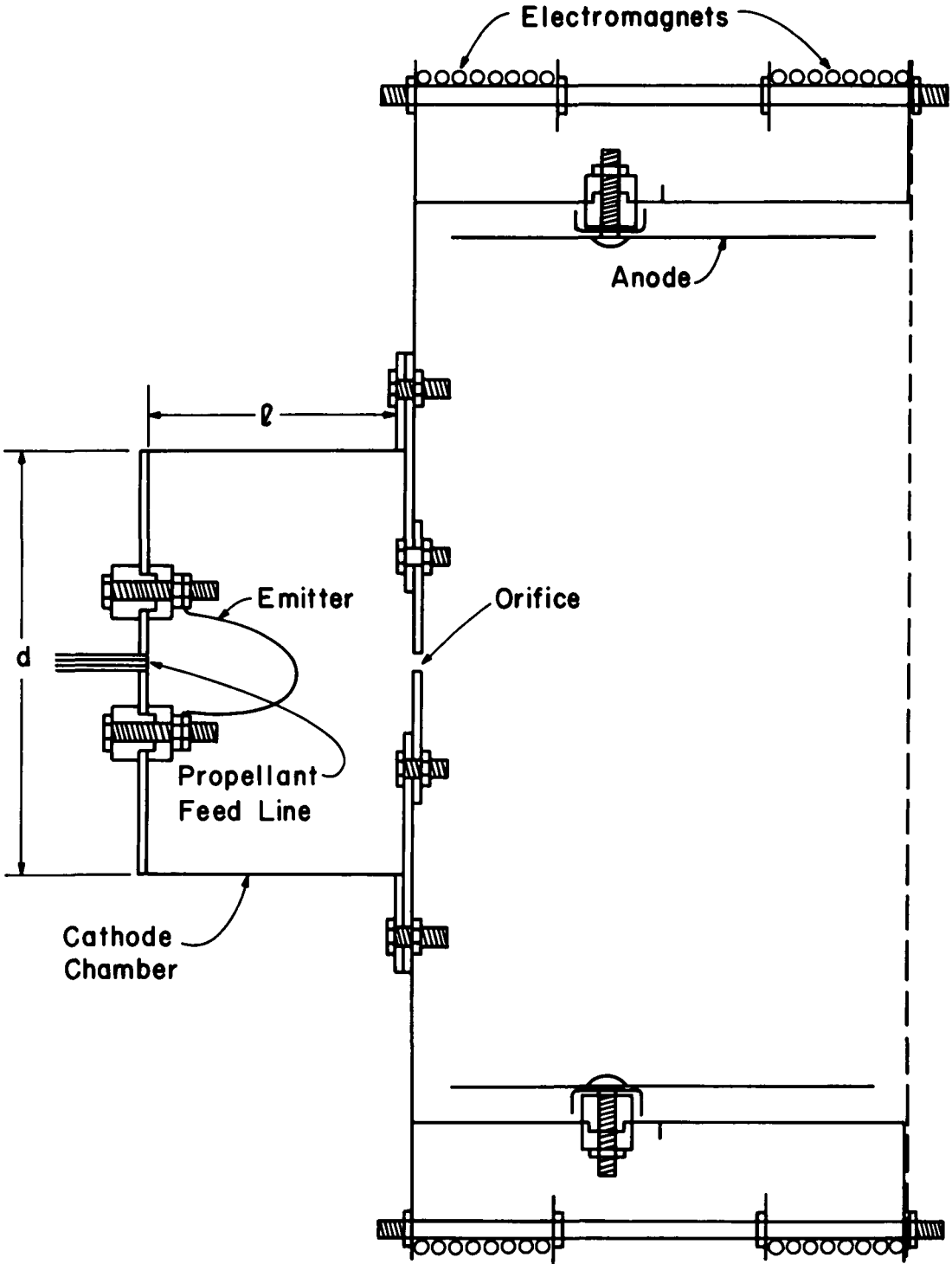

Figure 3. Sketch of hollow cathode and discharge chamber assembly.

about 3.8 cm. Tungsten wire with a diameter of 0.25 mm was used for all emitters. Emitter length was 3.5-4.0 cm except for the 0.64 cm cathode chamber diameter, which used a 2.5 cm length. The emitter connections were made through the back (upstream) wall in all configurations except the 0.64 cm diameter, where the connections were made in the side (cylindrical) wall. Propellant feed was through the back wall in all tests. In most configurations the orifice plate was 1 mm thick tantalum, 5 cm in diameter. Eight mounting screws permitted the rapid replacement of this plate for a change in orifice hole size.

Cathode discharge currents were limited in this study to less than about 5 amperes. This level is sufficient for a main discharge of a 15-20 cm source, or the neutralizer of a 30 cm source.

All the orifice plates were 1 mm thick. This thickness was found to be an approximate minimum value for both conducting away heat and withstanding erosion in mercury hollow cathodes. (A larger thickness than the minimum value is not desirable because of increased ion recombination within the orifice.) If similar voltages were obtained with argon, the heat losses and erosion rates would be roughly the same as mercury, hence require about the same minimum thickness. Because similar voltages for argon and mercury are implied in the long-life objectives of this study, initial investigations were limited to this 1 mm thickness.

IV. TEST ENVIRONMENT EFFECTS

The effect of bell jar pressure, P_{bj}, on cathode performance is shown in Fig. 4. The pressure difference was due to the use of two different vacuum facilities, as discussed earlier. The cathode configuration used was similar to that shown in Fig. 3, with the circuit the same as Fig. 2(a) except that no keeper was used. Although the orifice diameter and flow rates were not the same, the difference in discharge characteristics was typical for the two facilities. Most data were obtained in the lower pressure facility and typically showed the same sharp rise in voltage at some discharge current.

Cathodes were operated both with the simulated thruster as indicated in Fig. 3 and with an additional 7-mesh/cm stainless-steel screen anode (indicated schematically in Fig. 2(b)) to simulate neutralizer operation. When used, the screen was electrically connected to the cylindrical anode in the thruster simulator and the magnet current turned off. The screen was about 5 cm square and located about 2.5 cm downstream of the cathode (or keeper, when used).

The effect of using the screen anode is shown in Fig. 5. A non-zero bias voltage, V_b, was used, but the results shown in Fig. 5 are typical for all comparisons of data with and without screen anodes. The use of a screen anode resulted in higher discharge currents at all discharge voltages. The decreased anode-cathode distance and the absence of a magnetic field (or decreased strength thereof) probably contributed to the current increase with a screen anode. Part of the increase may also be due to an increase in pressure upstream of the

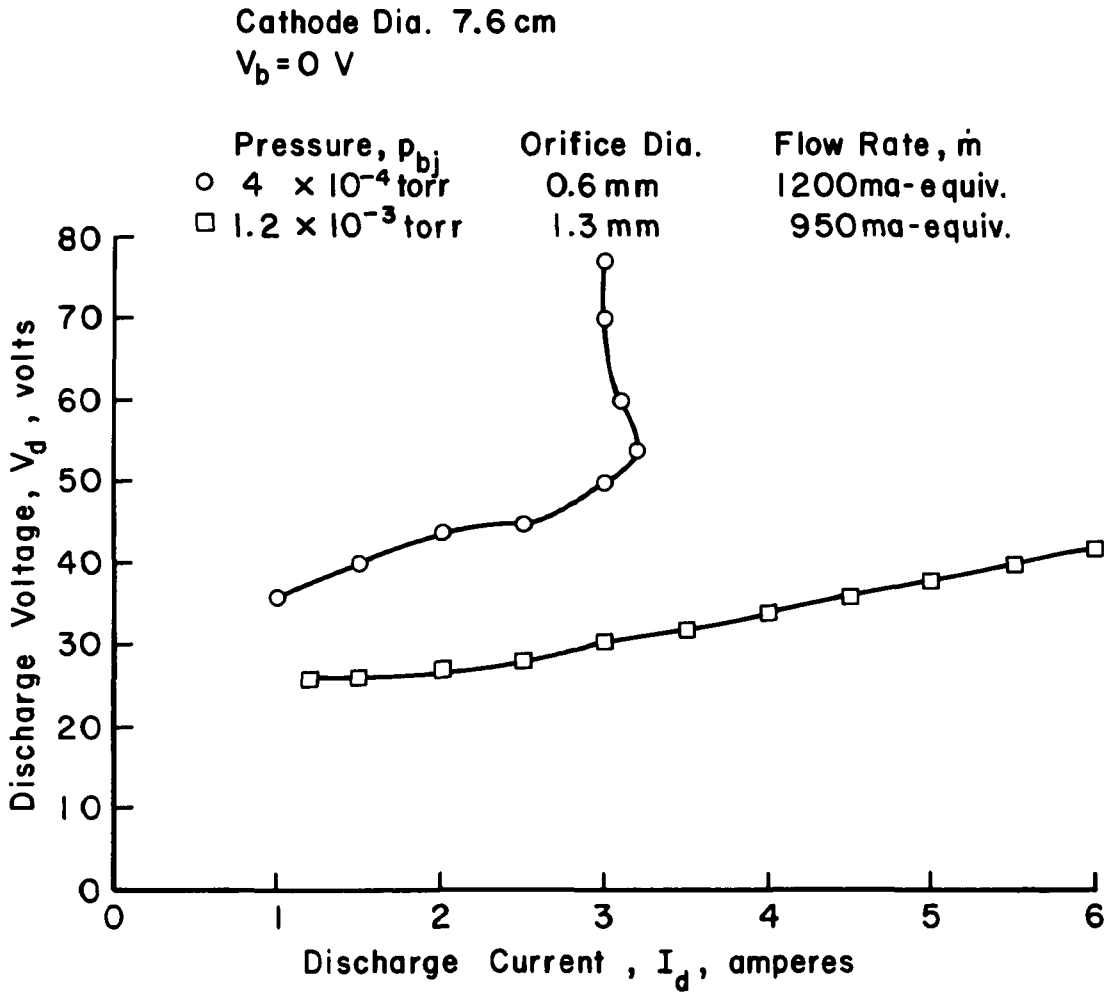

Figure 4. Effect of bell jar (background) pressure on cathode performance. Without screen anode.

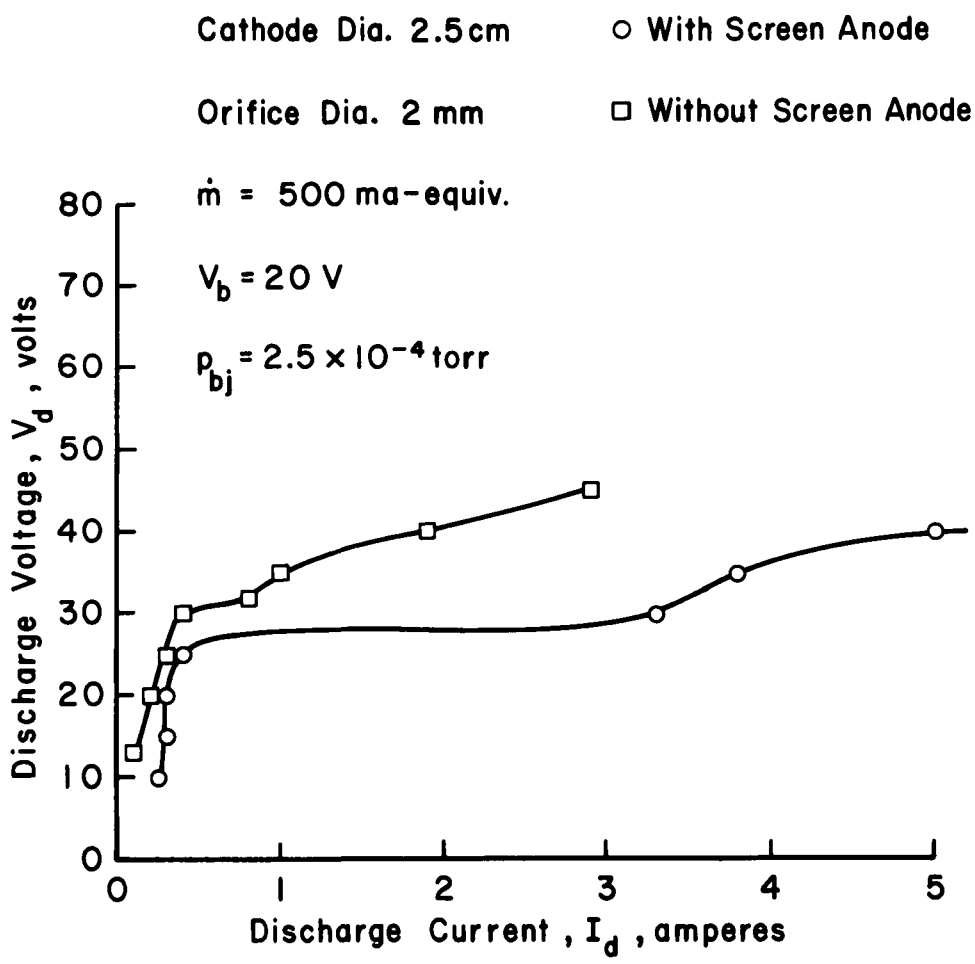

Figure 5. Effect of using a stainless steel screen anode, located 2.5 cm from the orifice vs. a conventional discharge-chamber anode.

screen, but this effect should be small because the open area fraction of the screen used was nearly 0.7.

Long life cathodes require low discharge voltages. It is true that discharge chamber potential differences of 40-50 volts may be required for efficient ionization, but the immediate environment of the cathode should be much closer to cathode potential if a long life is to be obtained. There is no "pole piece" or equivalent cathode protection in the simulated thruster of Fig. 3. Lower voltage operation at the same discharge current is therefore more desirable or better for the cathode. The terms "better" or "best" will be used throughout to describe such a voltage decrease. The incorporation of cathode protection into an actual thruster (such as a cathode pole piece) is important, but it is less pressing than the development of the cathode.

Emission calibration proved to be a recurrent problem. Tungsten wire of a constant diameter was used in all tests, with the emitter length the same in all except the smallest cathode chamber diameter. It was initially hoped that these precautions, together with the use of a constant heater current would serve to provide a constant emission. But sufficient emitter erosion (due to ion bombardment and/or the effects of impurities initially present) occurred so that constant heating current resulted in substantial increases in electron emission during some of the tests.

As the next calibration technique, a bias discharge between the emitter and cathode chamber wall was utilized. After establishing an internal discharge, the emitter bias voltage was reduced until the discharge was extinguished. The discharge was then re-established with the bias 5 volts above this minimum value for a discharge. The emitter

heater current was then adjusted until the emission was some standard value, typically 1 ampere. This calibration approach was an improvement over the use of a constant heating current through a constant length cathode. But it still had several shortcomings. In some cases, the internal discharge would slowly dwindle to zero as bias voltage was reduced, leaving no clear reference point for calibration. The variation of internal discharge with emitter heater current is shown in Fig. 6. Note that the minimum bias voltage for a discharge varies with heater current.

As a final calibration method for this study, entire emitter performance curves were taken -- as shown in Fig. 6. An initial curve at 7 amperes heating current served as a calibration for each configuration. As time passed during each run, these data were retaken and the heating current adjusted to give a discharge curve close to the original one obtained at 7 amperes. It is felt that this procedure corrects for most of the changes in emission that would otherwise take place with time.

Another test environment problem was the appearance of a thin, insulating layer on the interior surfaces of the thruster simulator, particularly the anode. The problem was probably due to the presence of foreign material, such as residual oil, on the thruster components. The coating seemed to appear immediately after the installation of new components into the system. Removal of the coating required manual cleaning for the first 2 or 3 runs, but subsequent tests could be conducted without any problem. The coating had a resistance as high as a megohm and the effects on cathode operation are shown in Fig. 7 for two different bias voltages. (Non zero bias voltages are discussed

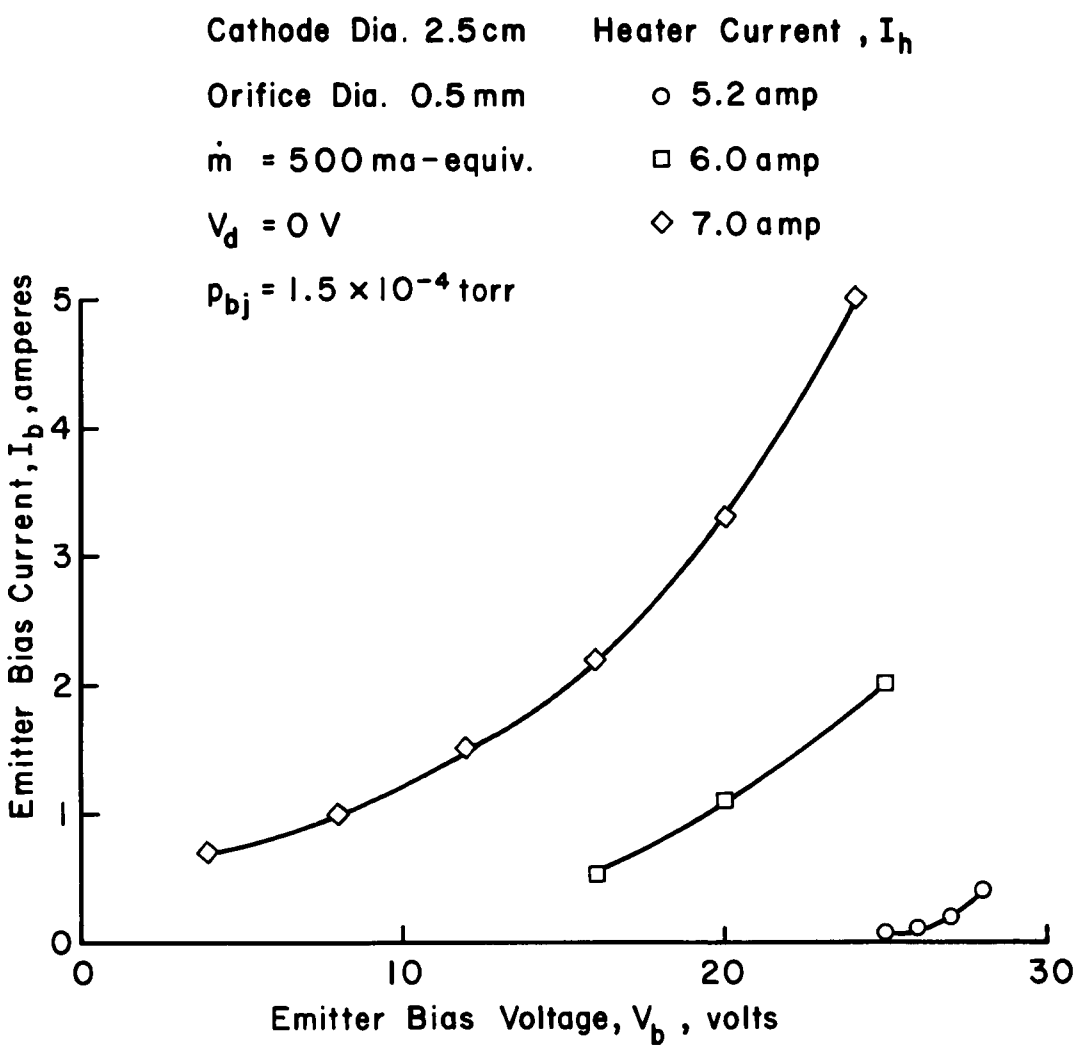

Figure 6. Effect of heater current changes on cathode emission. Without screen anode.

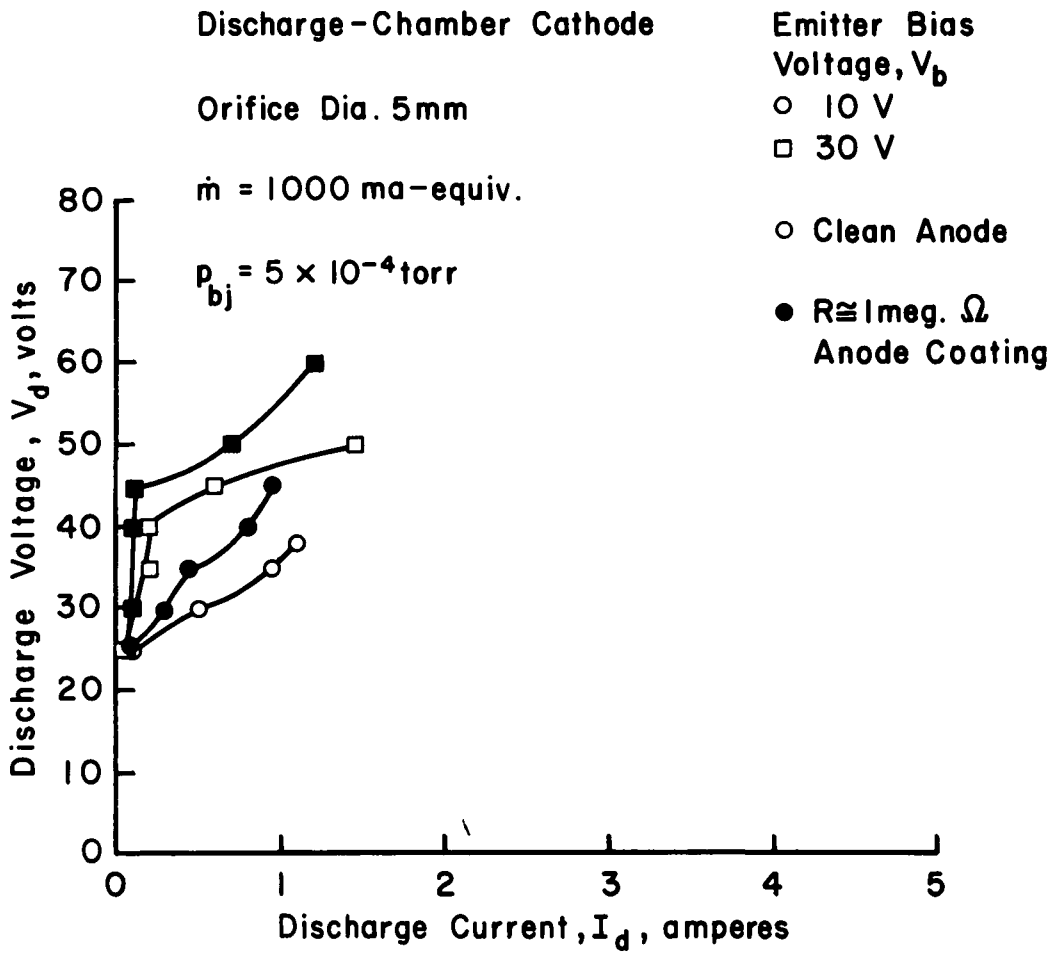

Figure 7. Performance comparison with and without resistive coating on the anode.

later.) Performance is poorer with the anode coating but perhaps not as bad as what might be expected for such a high resistance. The problem was not particularly acute, however, and the bulk of the tests were conducted with no coating problems.

V. EXPERIMENTAL RESULTS

Cathode Size Effect

Inasmuch as both volume and surface losses tend to increase with plasma size, cathode performance was expected to improve with a decrease in cathode chamber size. The initial intent of the size investigation was to determine the penalty for a size increase. A size increase over the usual 3 and 6 mm diameter mercury hollow cathodes would, of course, ease fabrication problems for more complex geometries, as well as provide more radiation area for cooler operation.

The results of varying cathode chamber diameter are shown in Fig. 8. Instead of the expected monotonic improvement in performance with decreased size, a broad optimum was found from about 1 to 2.5 cm in diameter. The nearly horizontal curves of the intermediate diameters would, from other data, be expected to show sharp rises in voltage if they had been extended to higher discharge currents. The 2.5 cm data apparently shows the beginning of this expected rise at 5 to 6 amperes of discharge current.

The cathode chamber length was kept nearly constant at 3.5 to 4 cm as mentioned earlier. The 0.64 cm diameter chamber therefore had a large length-to-diameter ratio. To make sure that this large ratio was not the cause of poorer performance of this diameter, an additional test (not shown) was conducted with the length cut in half. No significant performance difference was found for these two lengths of 0.64 cm diameter.

From Fig. 8, then, it appears that argon hollow cathodes should be larger in diameter than the sizes customarily employed for mercury

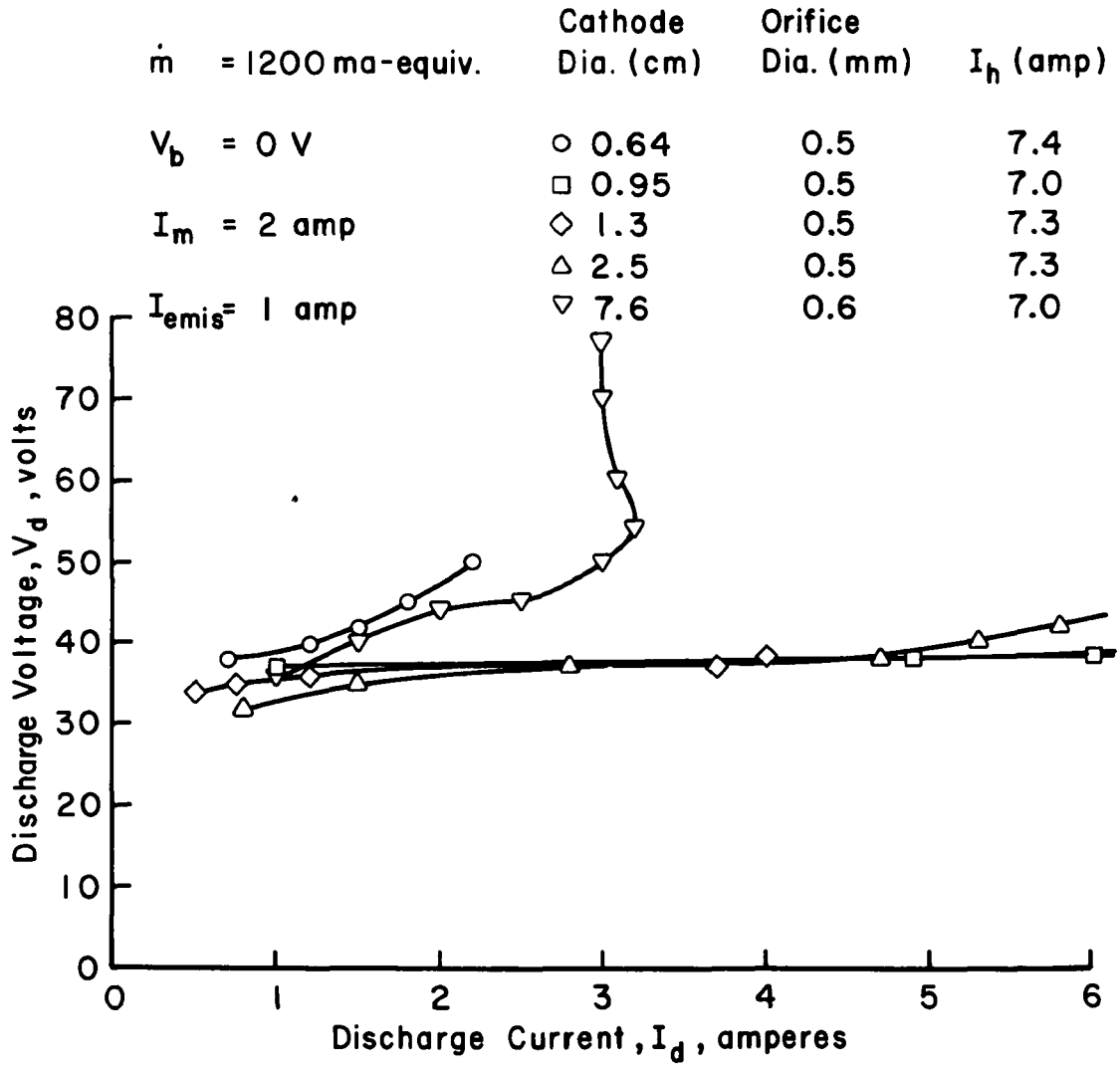

Figure 8. Survey of cathode performance as a function of cathode chamber diameter. Without screen anode.

hollow cathodes. This result is significant in that room can be made available for more complex electrode geometries without paying a performance penalty for the increased size. On the other hand, all the data in Fig. 8 were obtained at discharge voltages above 30. From endurance tests of hollow cathodes, a substantial reduction of discharge voltage would be required for the orifice of an argon hollow cathode to have thousands of hours of life.

Enclosed Keeper

Several modifications to the basic design were investigated as possible means for reducing the discharge voltage. The use of an enclosed keeper was one of these modifications. Ions striking the emitter with energies above 30 eV would cause too much erosion to obtain long lifetimes.[11] Hopefully, the enclosed keeper would decouple the emitter from such high energy ions.

A cathode diameter of 0.64 cm was selected because promising results had been obtained at the NASA Lewis Research Center in preliminary tests with this size using an enclosed keeper and an oxide-impregnated insert. These preliminary tests were obtained with the cathode operating as a neutralizer, so the screen anode was used herein to simulate neutralizer operation.

Data obtained with an enclosed keeper are shown in Fig. 9. The discharge voltage remained above 30 with a keeper, while no significant increase in discharge current was found. In fact, an increase in the keeper current resulted in a decrease of maximum discharge current. The keeper tended to float at about 12 volts. As the keeper voltage (V_K) was increased to 16 volts, the maximum discharge current was decreased by about the increase in keeper current.

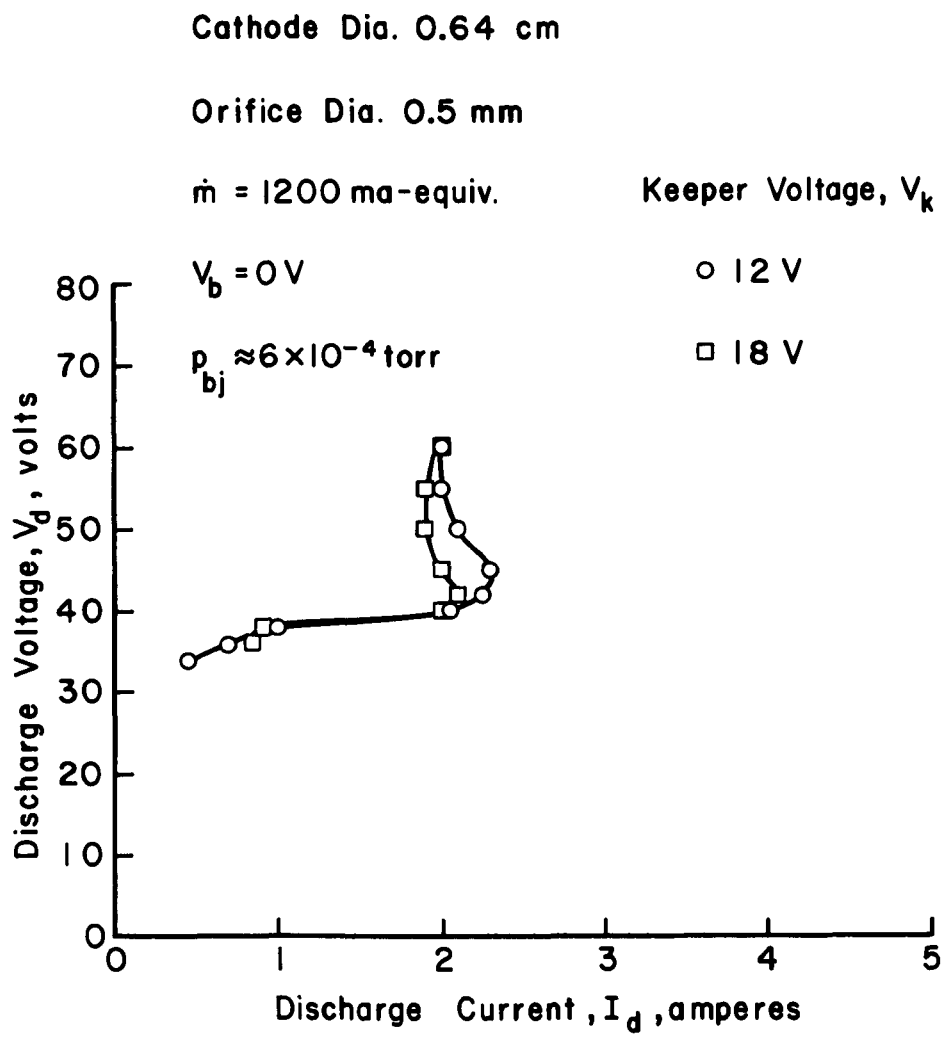

Figure 9. Performance with an enclosed keeper. The keeper was 1.3 cm from the cathode and had an orifice diameter of 0.76 mm. With screen anode.

The performance with a keeper was disappointing in that all operation was above 30 volts. This result differed sharply from performance obtained at NASA Lewis Research Center. The only significant difference in configuration appeared to be the use of a refractory emitter instead of an oxide-impregnated insert.

Effect of Barium-Strontium Oxides

Operation with an enclosed keeper, described above, resulted in substantially higher voltages than given by Mirtich. Because the presence of oxides appeared to be the only significant difference, tests were conducted herein with a commercial barium-strontium oxide mix (R-500, J.T. Baker Chemical Co.). A small amount of this mix was injected (as carbonates with a volatile carrier) into the 0.64 cm cathode chamber near the orifice.

As shown in Fig. 10, the use of oxides resulted in a substantial increase in discharge current. The normal function of oxides is to decrease the surface work function,[10] thereby increasing the emission at a given temperature. But the thermionic emitter used herein operated at a high enough temperature to vaporize rapidly any barium-strontium oxides that contacted it. The major cause of the performance difference with oxides is suspected to be vaporized oxides mixed with argon, thereby providing a small fraction of low ionization potential atoms which increases plasma conductivity.[16]

It is tentatively suggested, then, that the lower voltages obtained at Lewis resulted from "seeding" the argon with barium-strontium oxides. Depletion of oxide impregnated inserts could be a problem if seeding is the cause of the performance difference--rather than some other parameter such as background pressure.

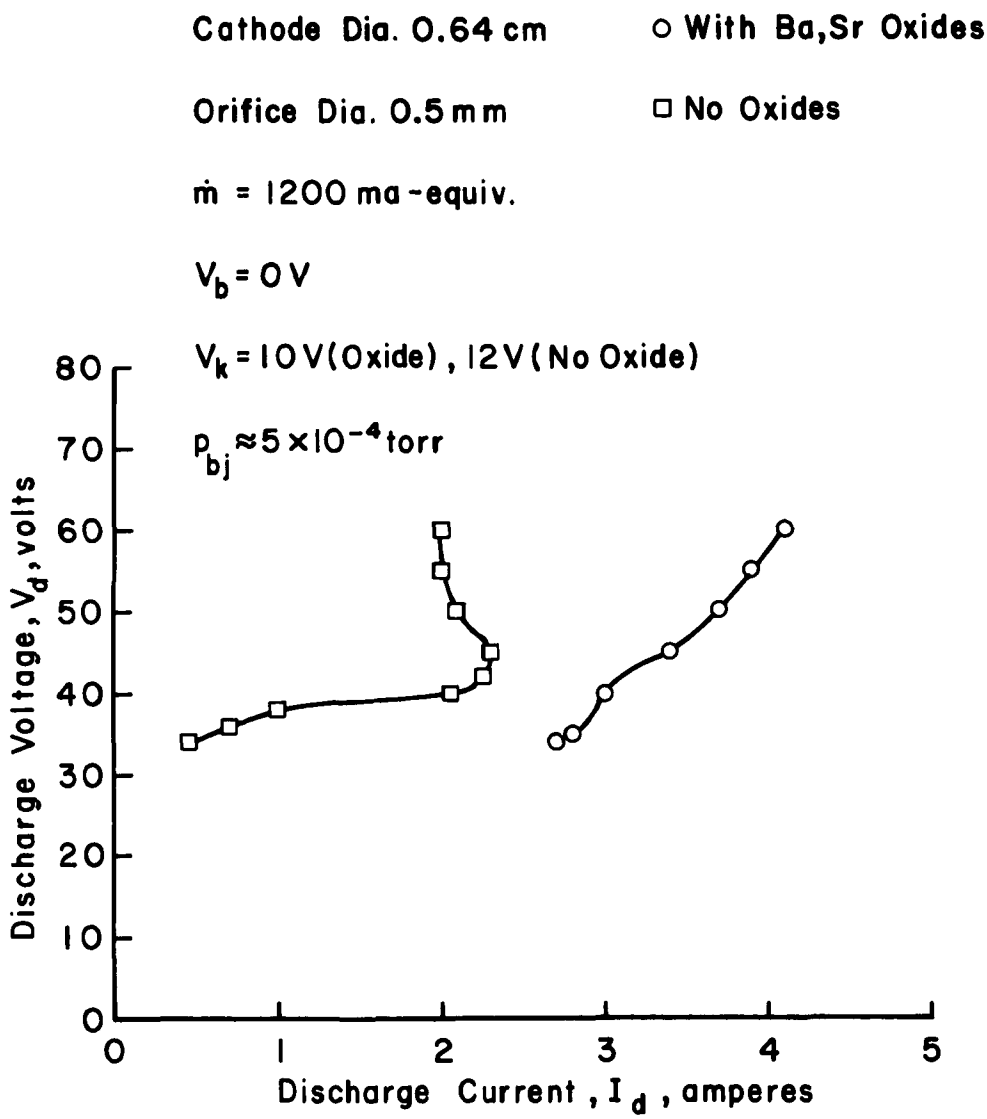

Figure 10. Performance comparison with and without barium-strontium oxides. With screen anode.

Comparison of Xenon and Argon

As mentioned at the beginning of the hollow cathode section, most tests were conducted with argon as the propellant. A few tests were conducted with xenon, though, for comparison with argon data. Data from these tests are shown in Fig. 11. The xenon performance curves have the same general shape as the argon curves shown previously. The specific performance values, however, are better for xenon. For example, xenon at 500 ma-equivalent has about the same corrected bell jar pressure as argon at 1000 ma-equivalent. But the discharge current varies over a wider range with xenon.

The better performance with xenon should be expected from the lower ionization potential, the larger ionization cross section, and the higher atomic weight. The latter results in a higher neutral density for the same ma-equivalent flow rate as argon. In general, wider ranges in discharge current are possible with xenon, while the discharge voltages are up to 10 V lower.

Orifice Size Effect

Another parameter investigated was that of orifice diameter. Figs. 12 and 13 show the effects of changing orifice size at high and low bell jar pressure. Although a screen anode is used for the low pressure data, the differences between Figs. 12 and 13 are similar to the differences shown for high and low pressure data in Fig. 4. The low pressure data should be more representative of a thruster environment, so that considerations of optimum orifice size will be restricted to Fig. 13. For discharge currents of 3 to 5 amperes, the 0.5 mm orifice resulted in the lowest discharge voltage. At lower discharge currents, the 2 and 5 mm orifices result in the lowest discharge voltages. It is

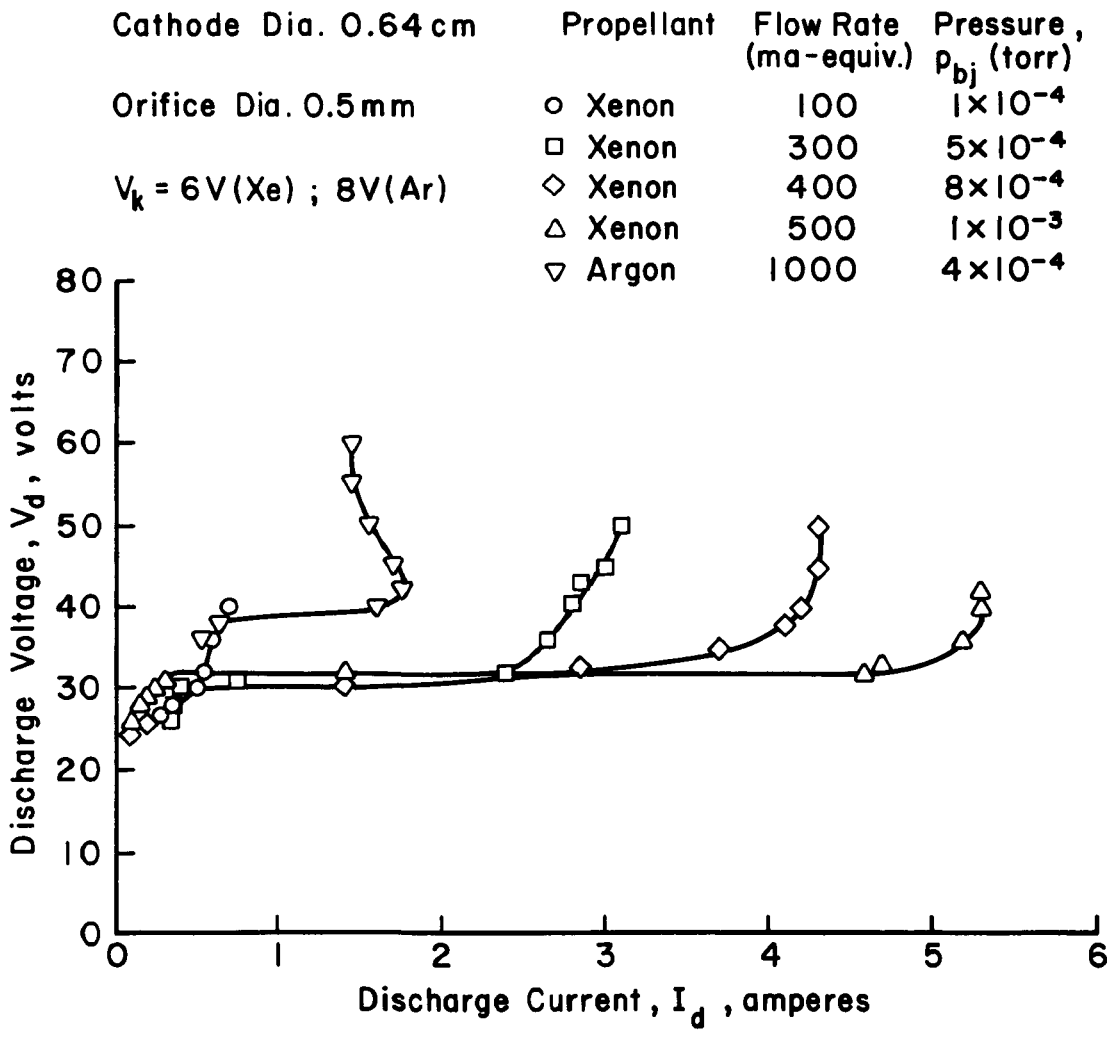

Figure 11. Comparison of argon and xenon performance with several flow rates of xenon used. With screen anode.

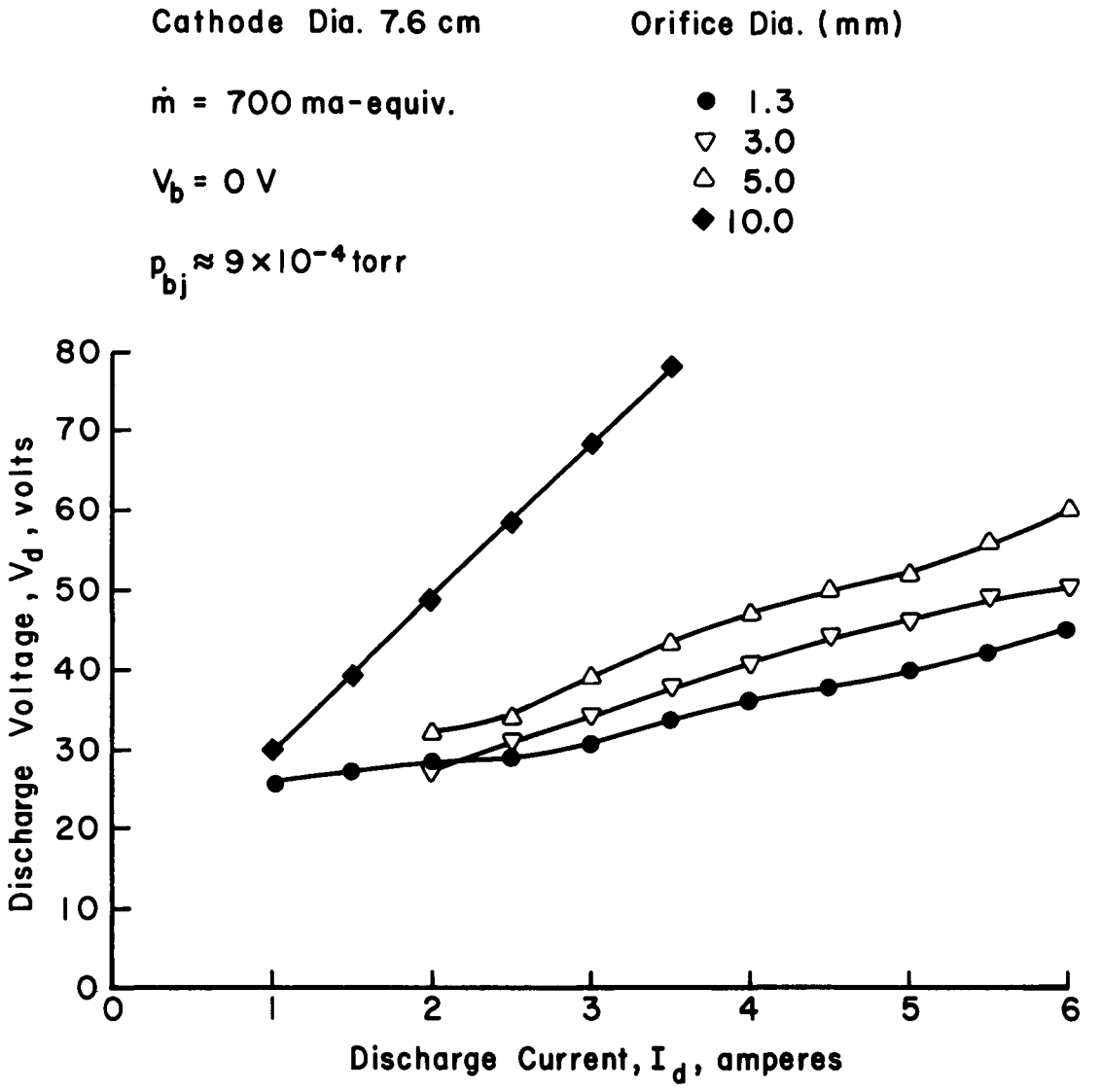

Figure 12. Effect of orifice size changes at high bell jar (background) pressure. Without screen anode.

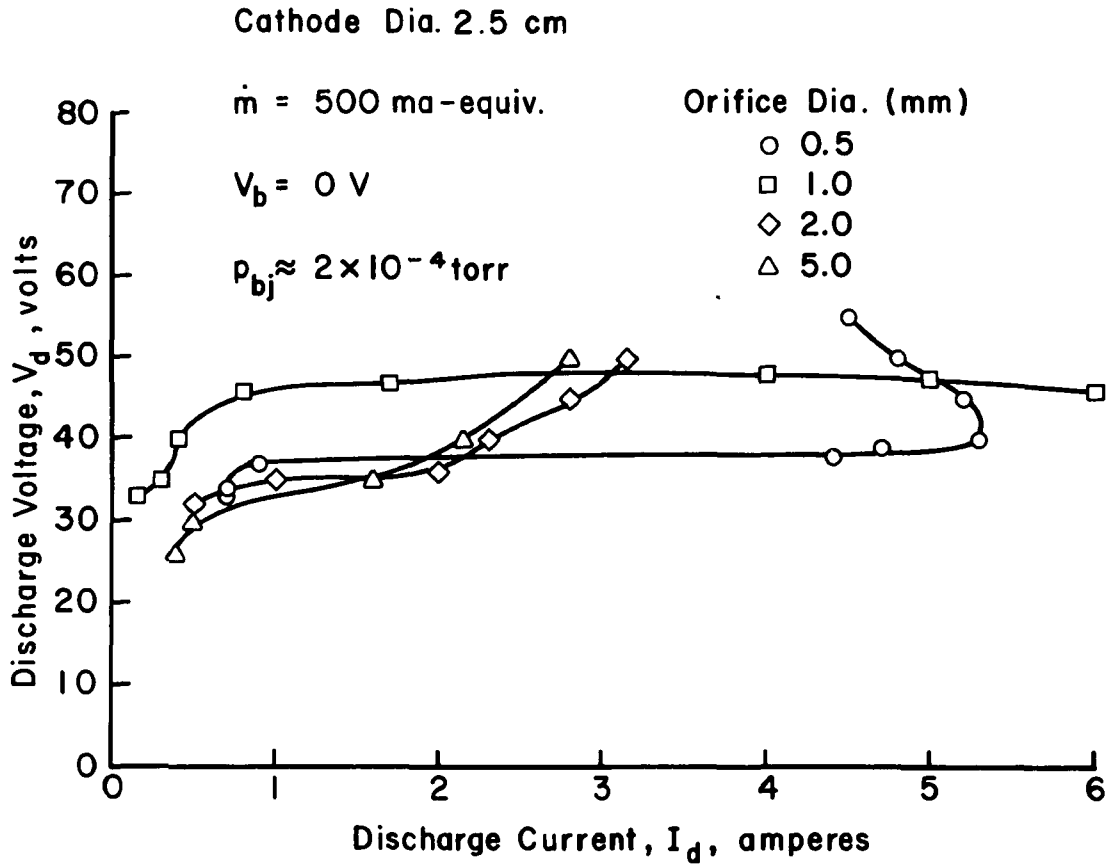

Figure 13. Effect of orifice size changes at low bell jar (background) pressure. With screen anode.

not clear why the 1 mm orifice has the highest discharge voltage over much of the current range. For comparison, a typical mercury hollow cathode uses an orifice diameter in the range 0.1-1 mm.[17]

It is interesting that fairly long life could be obtained for a cathode in the 1 to 2 ampere range despite the high voltage. As shown in Fig. 13, an orifice could start at 2 mm and wear to 5 mm without significant change in operating characteristics. There would be a large amount of sputtered material using such a design, but it could be used in any application that would permit this amount of sputtering.

Another survey of orifice diameters, in which a nonzero emitter bias was maintained, is shown in Fig. 14. Only the trends due to orifice size changes will be discussed here. The other effects of emitter bias will be discussed in the following section. The 2 and 5 mm orifices are better at low discharge currents, similar to the trends in Fig. 13. At higher currents, though, the 1 mm orifice is best. the 0.5 mm orifice operated over a restricted range that appears to correspond to only a part of the 0.5 mm curve in Fig. 13. Both voltage and current limited power supply modes were used to obtain discharge curves. It therefore seems unlikely that a power supply interaction would prevent the 0.5 mm orifice from operating over a wider range. But until more is known about the operation of the 0.5 mm orifice with a bias, the possibility of a power supply interaction cannot be ruled out.[18]

Emitter Bias Effect

With the exception of Figs. 7 and 14, all preceding data were obtained with the emitter at cathode chamber potential. (Nonzero biases were used only to initiate a discharge for these previous tests.) The

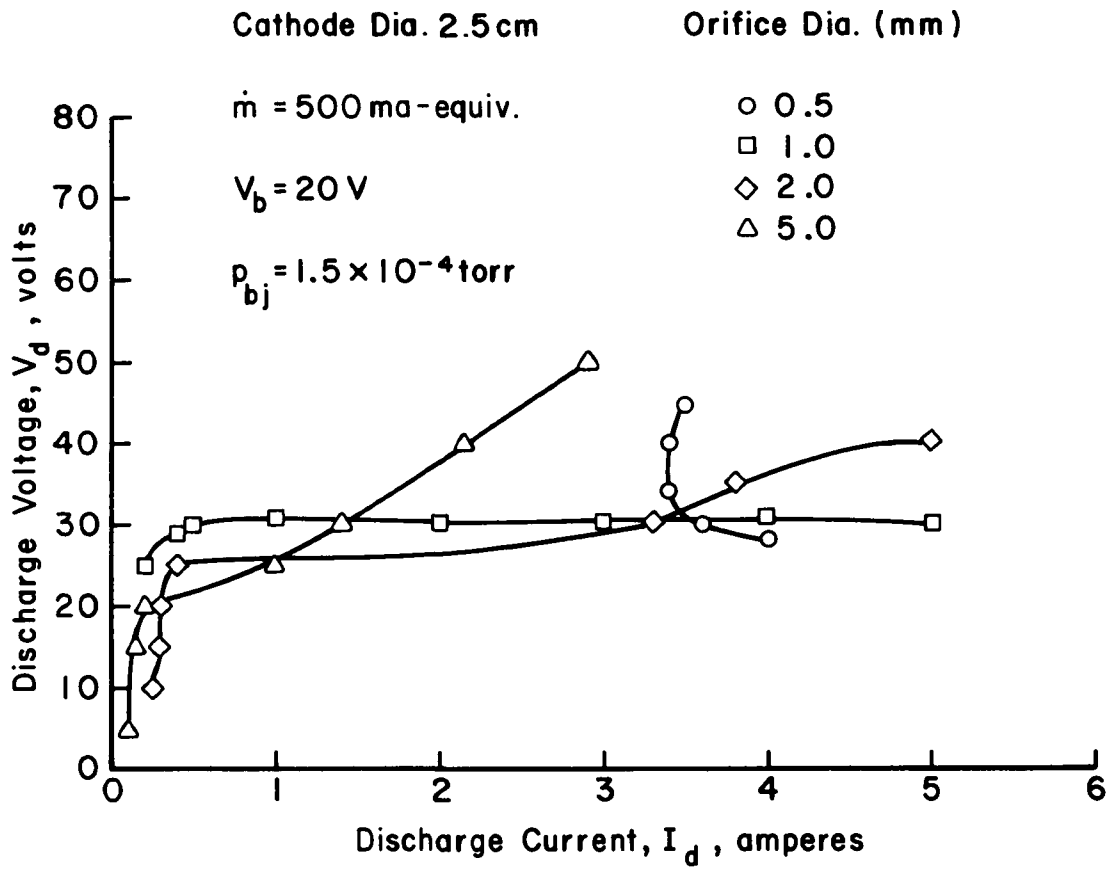

Figure 14. Effect of orifice size changes at a non-zero bias voltage. With screen anode.

effect of bias on steady state operation was investigated as a possible means of reducing discharge voltage, and hence erosion damage. Data from this portion of the investigation are shown in Fig. 15.

The effect of emitter bias voltage was substantial. Operation at discharge currents below 0.5 amperes was possible only with a bias voltage for the conditions shown. Above 0.5 amperes the use of a bias voltage permitted a substantial decrease in discharge voltage. The decrease in discharge voltage is clearly a step in the direction of decreased orifice sputtering. The effect on the emitter is less clear.

The discharge voltage is measured between the cathode chamber and the anode, while the emitter bias is between the emitter and the cathode chamber. The total emitter-anode voltage is therefore the sum of discharge voltage and emitter bias. The emitter lifetime will actually depend on the plasma environment in the cathode chamber, but this total voltage defines the approximate upper limit for energy ions that bombard the emitter.

The emitter-anode voltage can be increased or decreased by the use of a bias voltage, depending on the specific operating conditions. With a 10 V bias, for example, the emitter-anode voltage can be as low as 20 V (compared to a minimum of 32 V with no bias). On the other hand, the use of a 20 V bias at a 1 ampere discharge current gives an emitter-anode voltage of 47 V (compared with 35 V at the same discharge current and no bias).

From the emitter-anode voltage, then, the use of a bias voltage should lead to increased emitter lifetimes for some operating conditions. Plasma probe data and, ultimately, life tests will be required to

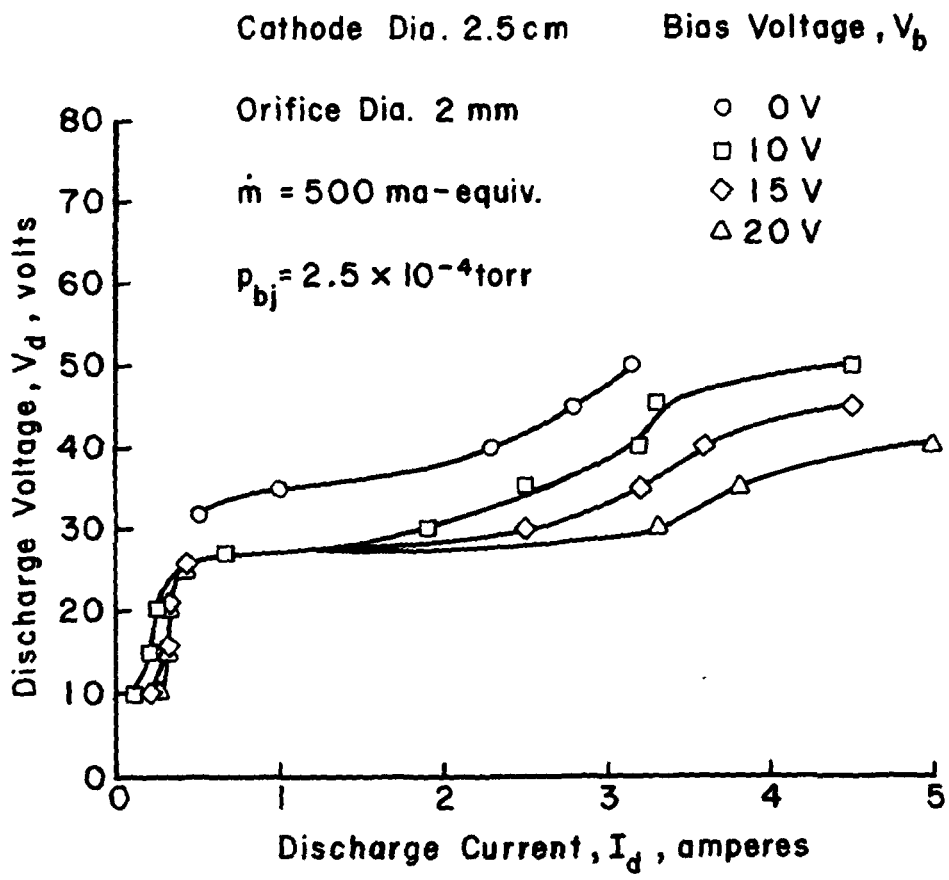

Figure 15. Effect of changes in emitter bias voltage. With screen anode.

determine the effect of emitter bias on emitter lifetime at other operating conditions.

Some other advantages of using a bias voltage are not shown in Fig. 15. While the minimum discharge voltage is 10 V in Fig. 15, bias data at other conditions showed minimum discharge voltages close to zero. Also, the minimum flow could be reduced from 500 ma-equivalent (no bias) to 200 ma-equivalent (with bias). With no coupling through the orifice, the internal bias discharge could be maintained at flows as low as 50 ma-equivalent.

A substantial electron current from the emitter to the cathode chamber wall was always observed during operation, even at zero bias voltage. The center tap of the emitter heating transformer winding was connected to the negative side of the bias supply. At zero bias, then, one side or the other of the emitter is negative relative to the surrounding chamber. With a conducting plasma present, an electron current will flow from the negative side of the emitter to the cathode chamber wall. The power supply requirements of the bias supply are indicated by data in Fig. 16, where both the internal bias discharge and external discharge characteristics are shown for a range of operating conditions.

Magnetic Orifice Cathode

The use of a magnetic field at the cathode orifice was included among the cathode concepts investigated to reduce discharge voltage. A sketch of the configuration used is shown in Fig. 17. The cathode chamber consisted of a nonmagnetic stainless steel tube that was 2.5 cm in diameter. The magnetic field at the orifice passed between a 6.4 mm diameter soft iron rod and a 1.6 mm thick orifice plate.

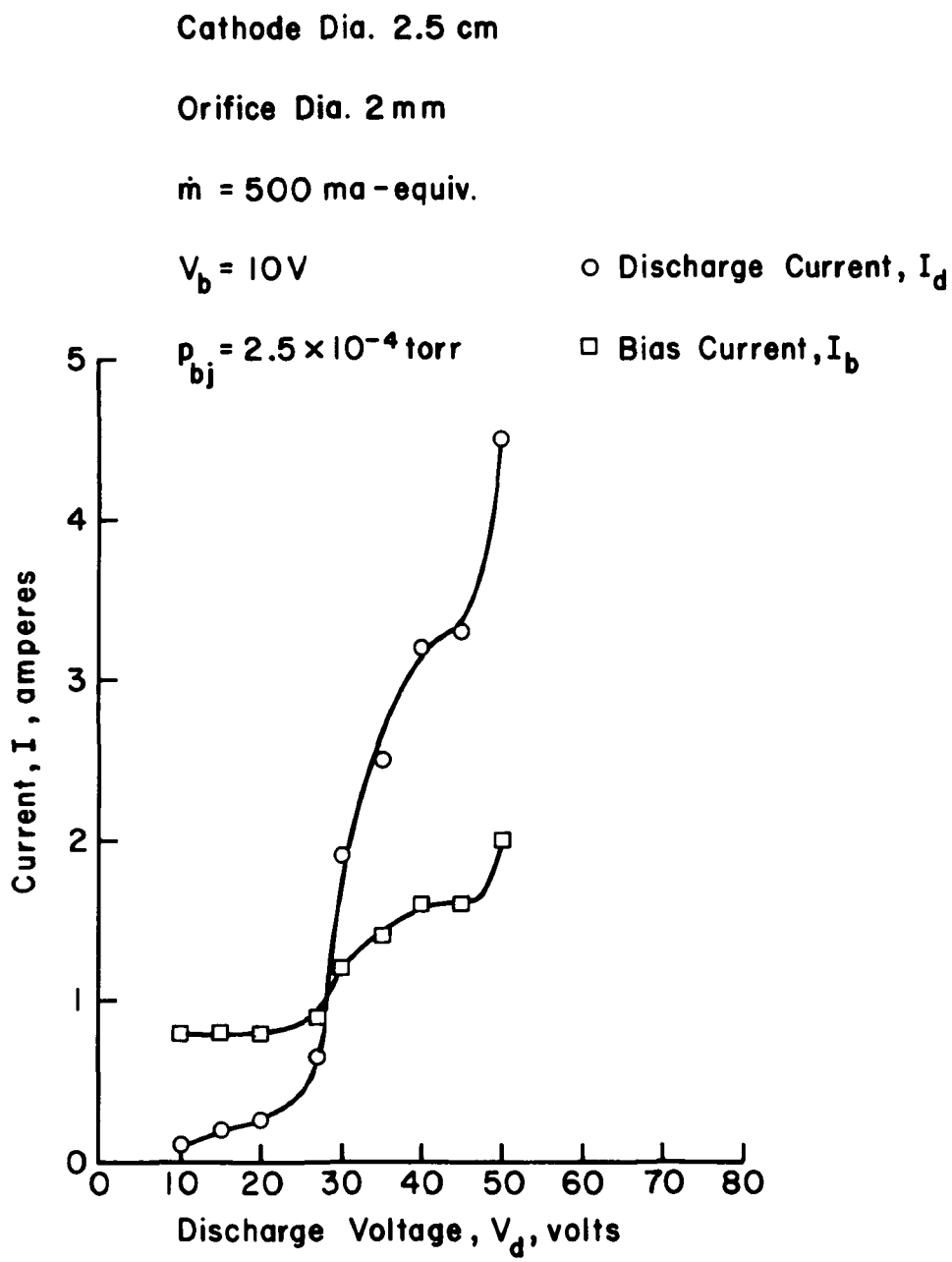

Figure 16. Comparison of discharge and bias current for the same operating condition. With screen anode.

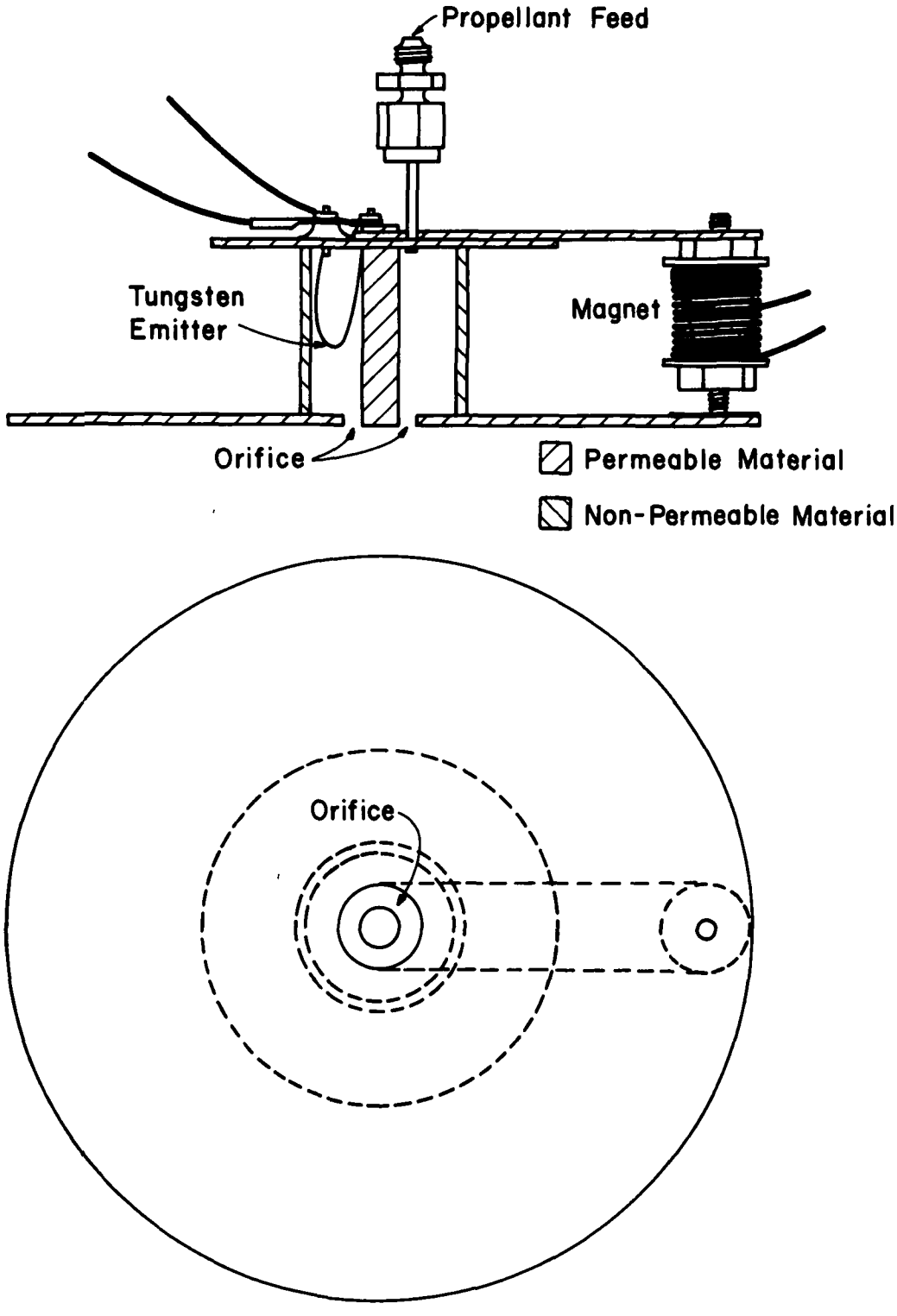

Figure 17. Magnetic orifice cathode.

Data obtained with the magnetic orifice cathode are shown in Fig. 18. The data with an annular orifice area of 0.95 cm^2 were obtained first. The performance was so poor that another orifice area (0.40 cm^2) was tried. The performance with the reduced area was substantially improved, but showed little advantage over the simple biased cathode of Fig. 15.

The field strength in the center of the orifice gap (0.40 cm^2 area) was about 150 Gauss at 3 amperes and something less than 50 Gauss at 0 amperes. Calculations indicated that $\leq$ 50 eV electrons should be contained at a maximum field strength of about 120 Gauss, so that the maximum experimental value of 150 Gauss should have been sufficient as the upper end of the range covered.

A magnetic field would be expected to reduce electron mobility through the orifice and increase ion production in that region. From the data of Fig. 18, though, the added ionization within the orifice due to a magnetic field has little effect on cathode performance. This conclusion is supported by the small difference between data obtained at 0 and 3 amperes. The big difference in data for the two orifice areas is probably due to pressure effects within the cathode chamber. Note that the 0.95 cm^2 annular orifice is equal in area to that of an 11 mm circular orifice.

Discharge Chamber Cathode

The construction of the discharge chamber cathode concept is indicated in Fig. 19. The magnetic field is provided by four 6.4 mm diameter permanent magnets between two permeable pole pieces. The strength of the magnetic field was sufficient to prevent 50 eV electrons from going directly to the internal anode after emission. The magnetic

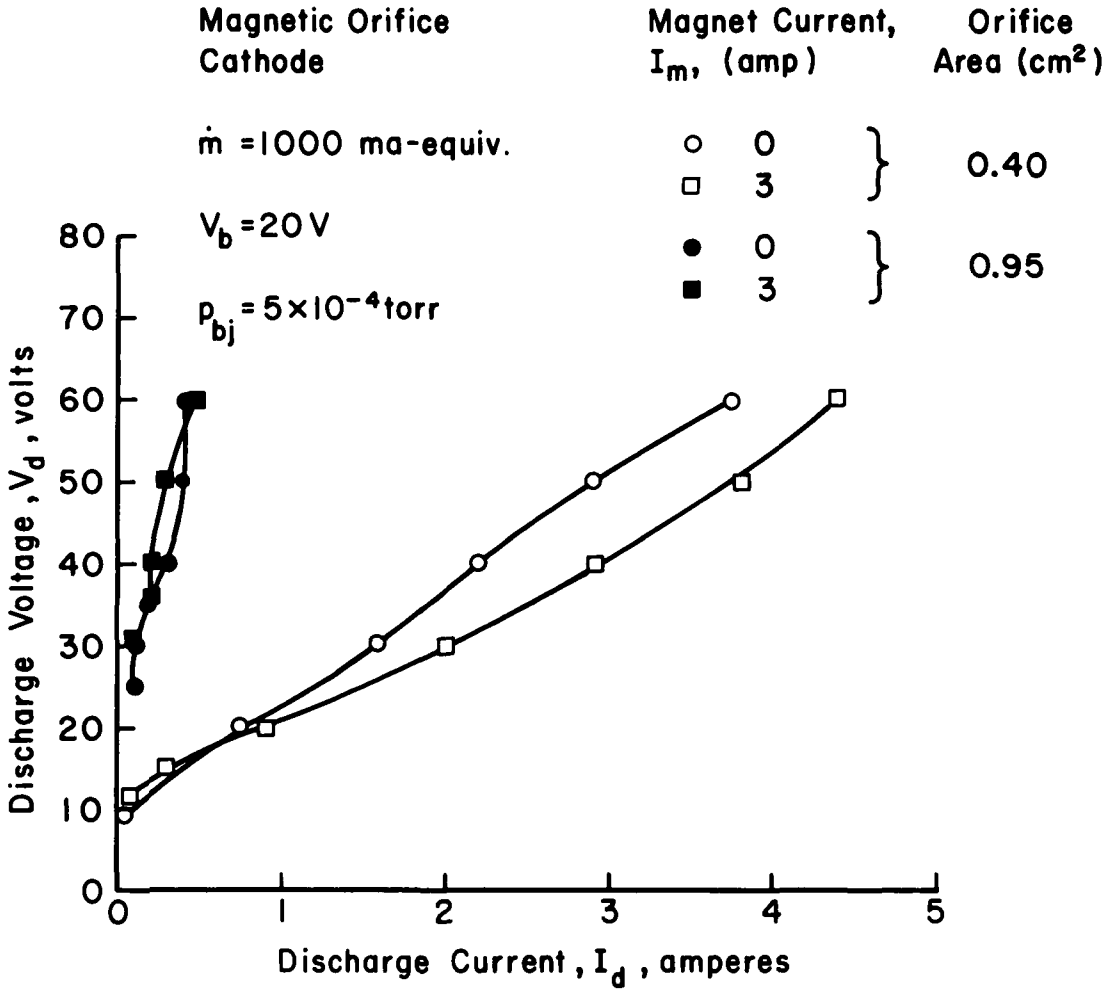

Figure 18. Effect on the performance of the magnetic orifice cathode due to changes in magnet current and orifice area. With screen anode.

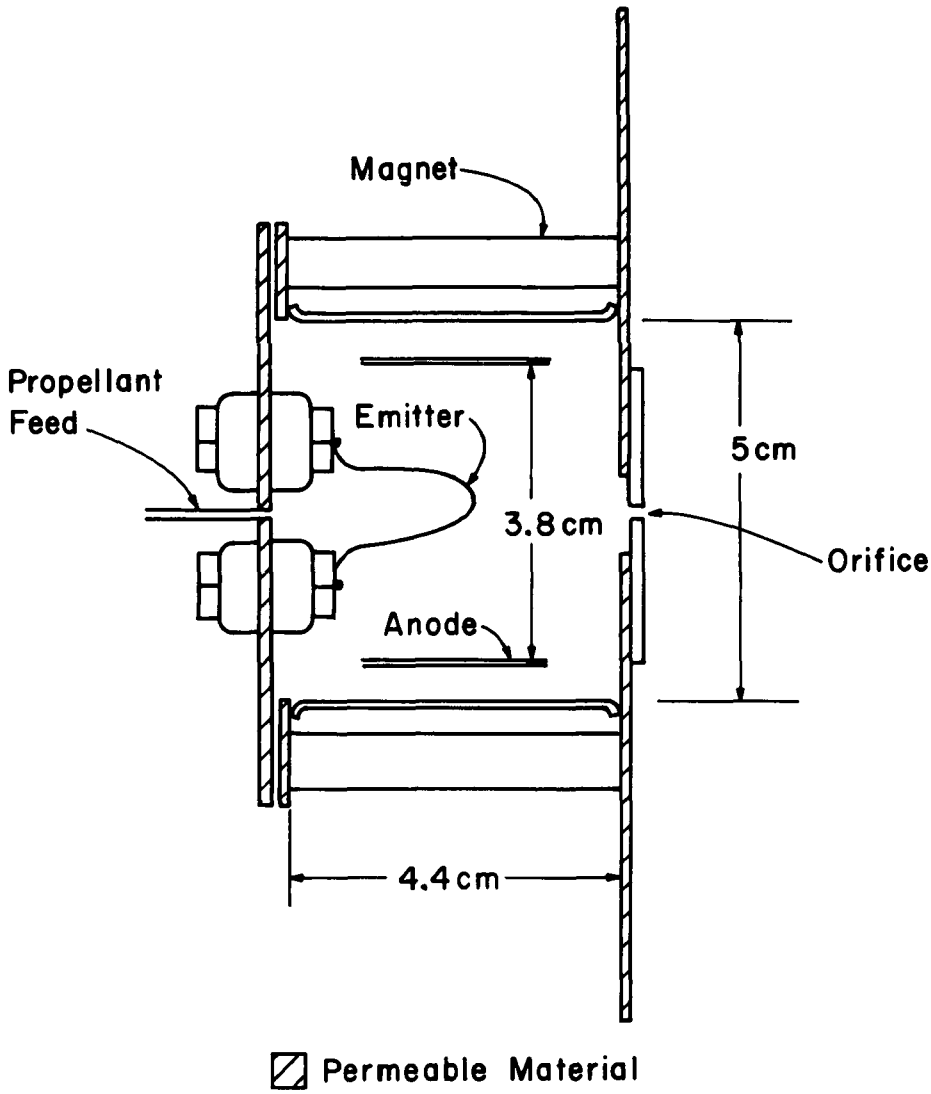

Figure 19. Discharge-chamber cathode.

field is slightly divergent due to the downstream pole piece being larger than the upstream one. This cathode is used in the electrical system indicated in Fig. 2(b). Note that the internal anode is biased relative to both the emitter and the cathode chamber. This means that the discharge voltage equals the emitter-anode potential difference, regardless of internal bias.

The performance of the discharge chamber cathode is shown in Fig. 20 for both 2 and 5 mm orifice diameters. (Operation was attempted with a 0.5 orifice, but the internal discharge could not be coupled to the external anode.) The discharge voltage generally increases with bias voltage for both orifice diameters. The difference is small, though,from 0 to 10 V bias. The advantage of a bias voltage for a simple cathode chamber (shown in Fig. 15) is therefore missing for the discharge chamber cathode. That is, the use of a bias voltage will not result in reduced orifice sputtering for a discharge chamber cathode.

The variation of emitter-cathode potential difference is a different story. In Fig. 15, for discharge currents that were common to both bias voltages, going from 0 to 10 volts bias resulted in 0 to 4 volts increase in emitter-anode voltage. For the discharge chamber cathode, keeping in mind the discharge voltage equals the emitter-anode voltage, the increase of the latter is 1 to 5 volts.

It appears that the use of a bias voltage can substantially change operating limits. But, within these operating limits, a bias of 10 V has little effect on emitter-anode potential difference. Also, for a bias voltage to reduce orifice sputtering, the emitter should be biased negative relative to the orifice. This means that a more

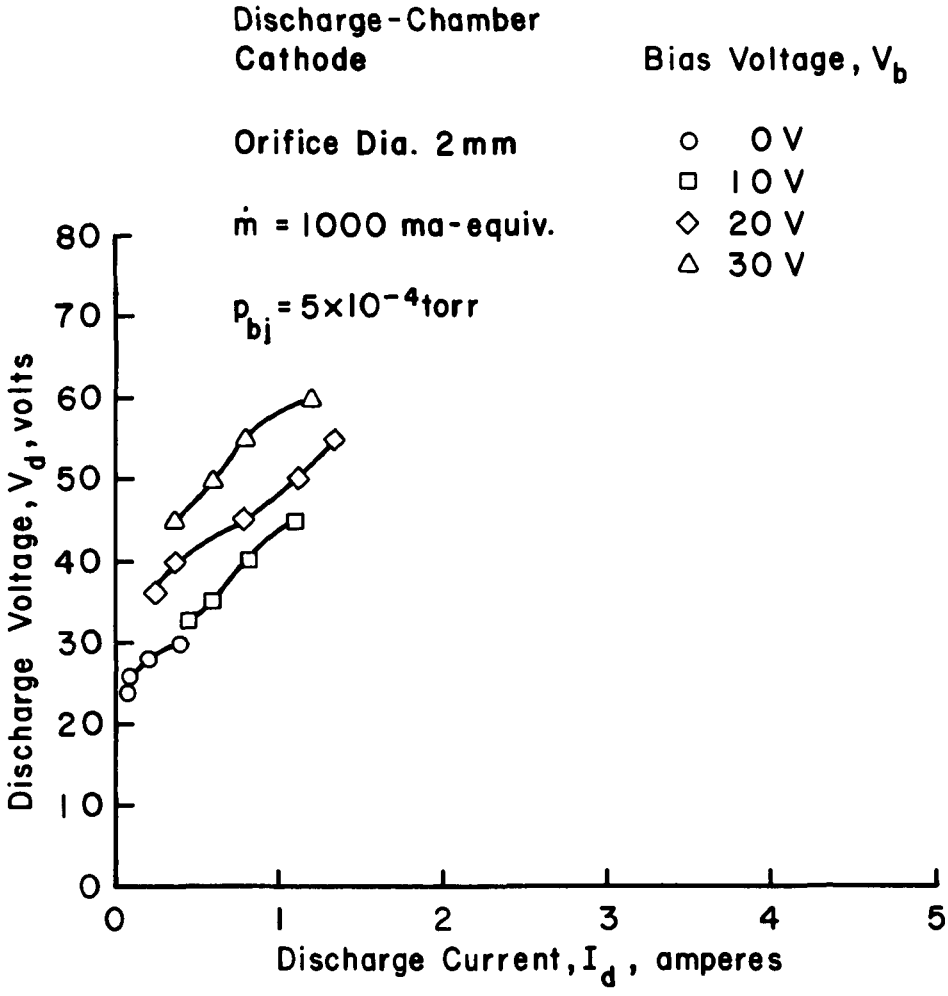

(a) 2 mm orifice

Figure 20. Effect of varying the emitter bias voltage on cathode performance. With screen anode.

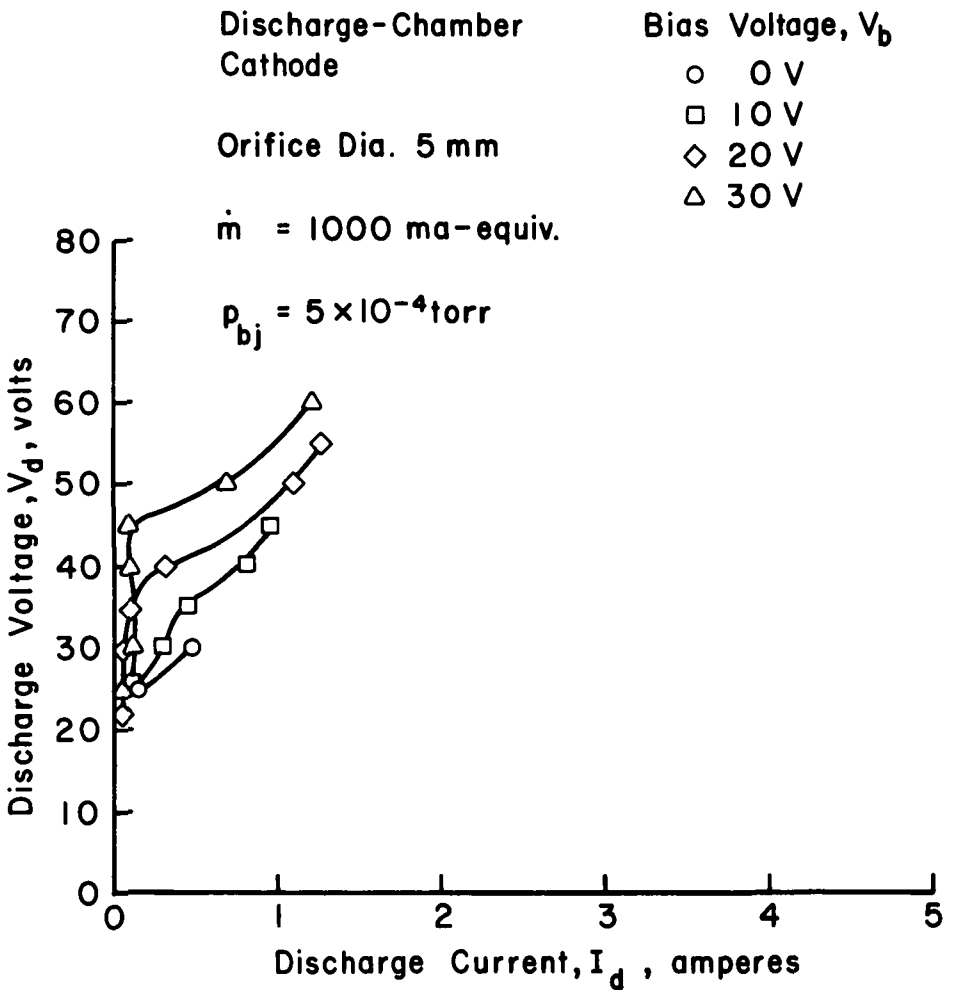

(b) 5 mm orifice.

Fig. 20. Concluded.

promising configuration of the discharge chamber cathode would have the orifice in the anode.

The effect of propellant flow rate on performance of the discharge chamber cathode is shown in Fig. 21, and is similar to that shown for other cathode types. The higher flow results in higher pressures and higher probabilities of electron collisions with atoms. The higher collision probability leads to lower discharge voltages.

Cathode Chamber Plasma Properties

Plasma properties within the cathode chamber were obtained using Langmuir probes.[19] The probe was an 0.07 mm diameter tungsten wire with an exposed area of about 1.3×10^{-2} mm^2. This probe was located 1 cm from the upstream plate of the 2.5 cm cathode chamber. The cathode performance data for the configuration used are shown in Fig. 22.

Plasma potential, electron temperature, electron density, and emitter bias current are shown as functions of discharge voltage in Fig. 23. At zero discharge voltage, the discharge current was also zero. The plasma properties at this condition were therefore the result only of the bias discharge. All the plasma properties change slowly with discharge voltage up to the 35 to 45 V range. Below this range, the plasma properties appear to be determined mostly by the internal discharge, and the plasma potential (relative to ground) is 5 V, or less. This means that ions from the internal plasma should strike the emitter at an energy corresponding to bias voltage plus 5 V, or 25 eV. The electron density is ~ 10^{14}/cm^3 (below a 35 V discharge), which is ~ 10^3 times more dense than a typical ion thruster discharge chamber. But the ion energy of 25 eV is approaching the sputtering

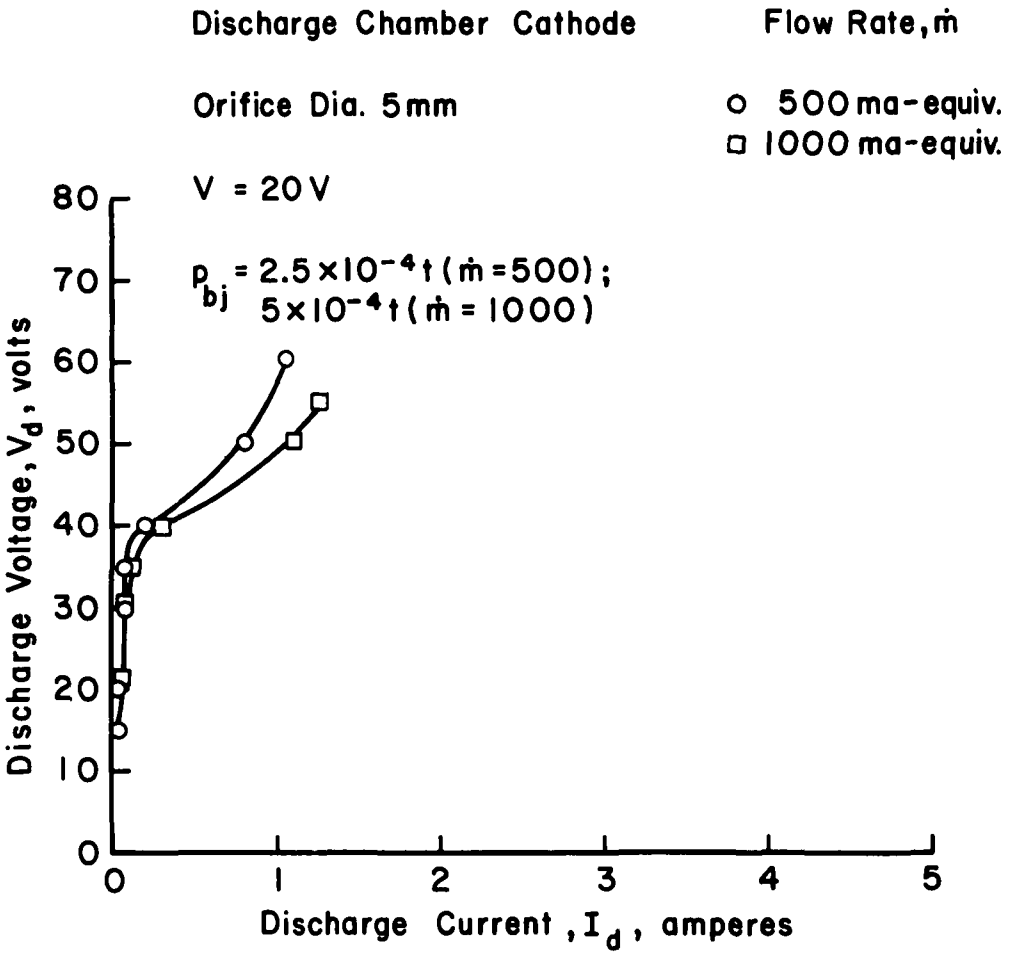

Figure 21. Effect of changing the propellant flow rate on cathode performance. With screen anode.

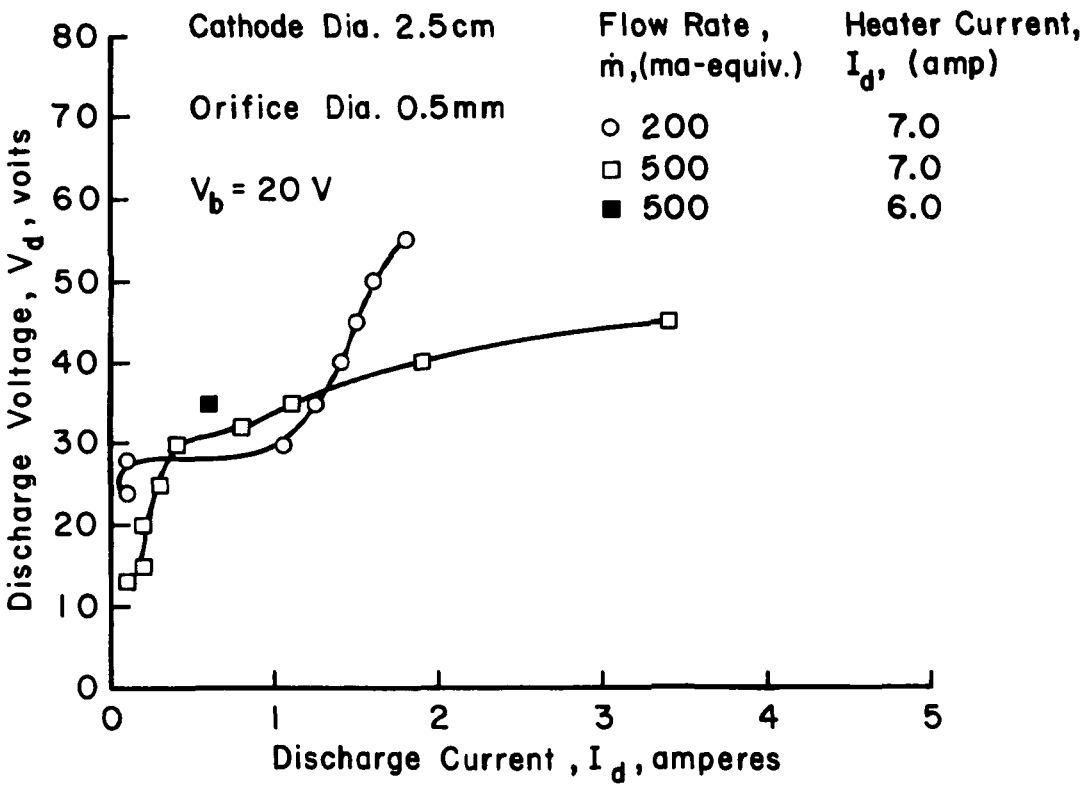

Figure 22. Cathode operating conditions corresponding to plasma properties illustrated in Figures 24-26. With screen anode. (Plasma properties not obtained at all data points.)

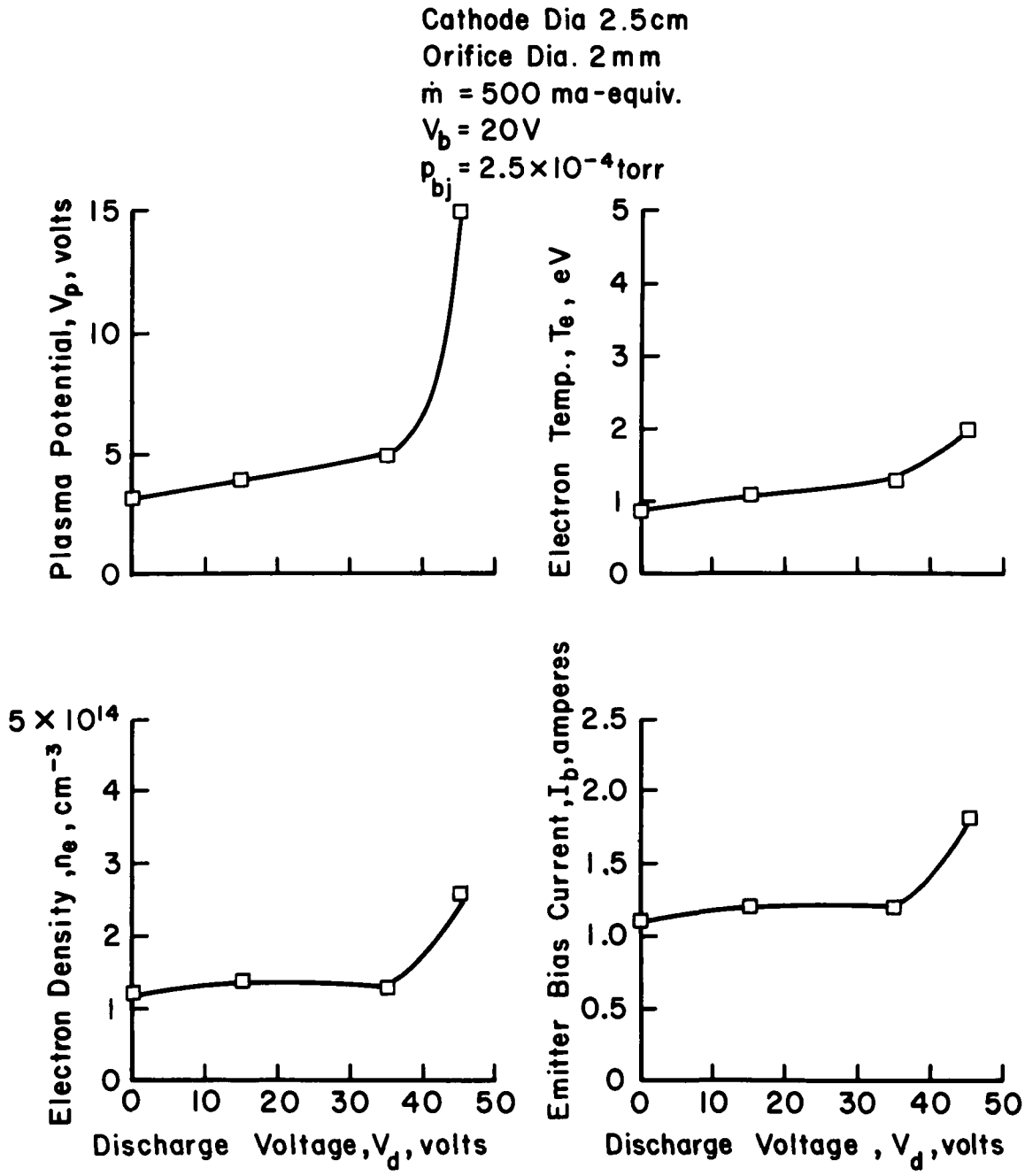

Figure 23. Plasma properties as a function of discharge voltage.

threshold, where indefinite lifetime can be expected in the absence of contaminants.[11]

The plasma properties are also shown in Fig. 24 and 25 as functions of propellant flow rate and emitter heater current. The effects of flow rate are minor, except for a small rise in plasma potential at the lower flow rate. The effects of decreasing the emitter heater current by one ampere is more significant. This decrease leads to a substantial reduction in emission, as indicated by the drop in bias current. This, in turn, results in a substantial drop in electron density. To offset the decrease in electron emission, the plasma potential increases. This increases ionization by increasing both the emitted electron energy and the background electron temperature. It is clear that an excess of electrons from the emitter is preferable to a shortage. A shortage will lead to higher energies for bombarding ions and therefore a more rapid failure of the emitter.

The effect of changing bias voltage was found to be more complex. Above 10 V, bias voltage changes resulted in little change of plasma potential or electron density. The electron temperature, surprisingly, decreased slightly with an increase in bias voltage. Below 10 V, probe traces became increasingly difficult to analyze. The effect of bias voltage on the probe trace is indicated in Fig. 26. These traces were obtained in a 2.5 cm cathode chamber with a 5 mm orifice.

Assuming a Maxwellian electron distribution, the probe current becomes nearly constant or increases slowly as the probe potential is increased above the plasma potential. Fig. 26(c), at 20 V bias, shows the curve shape normally expected, with a well defined inflection point at plasma potential (at ~ 30 V probe potential). At a 10 V bias,

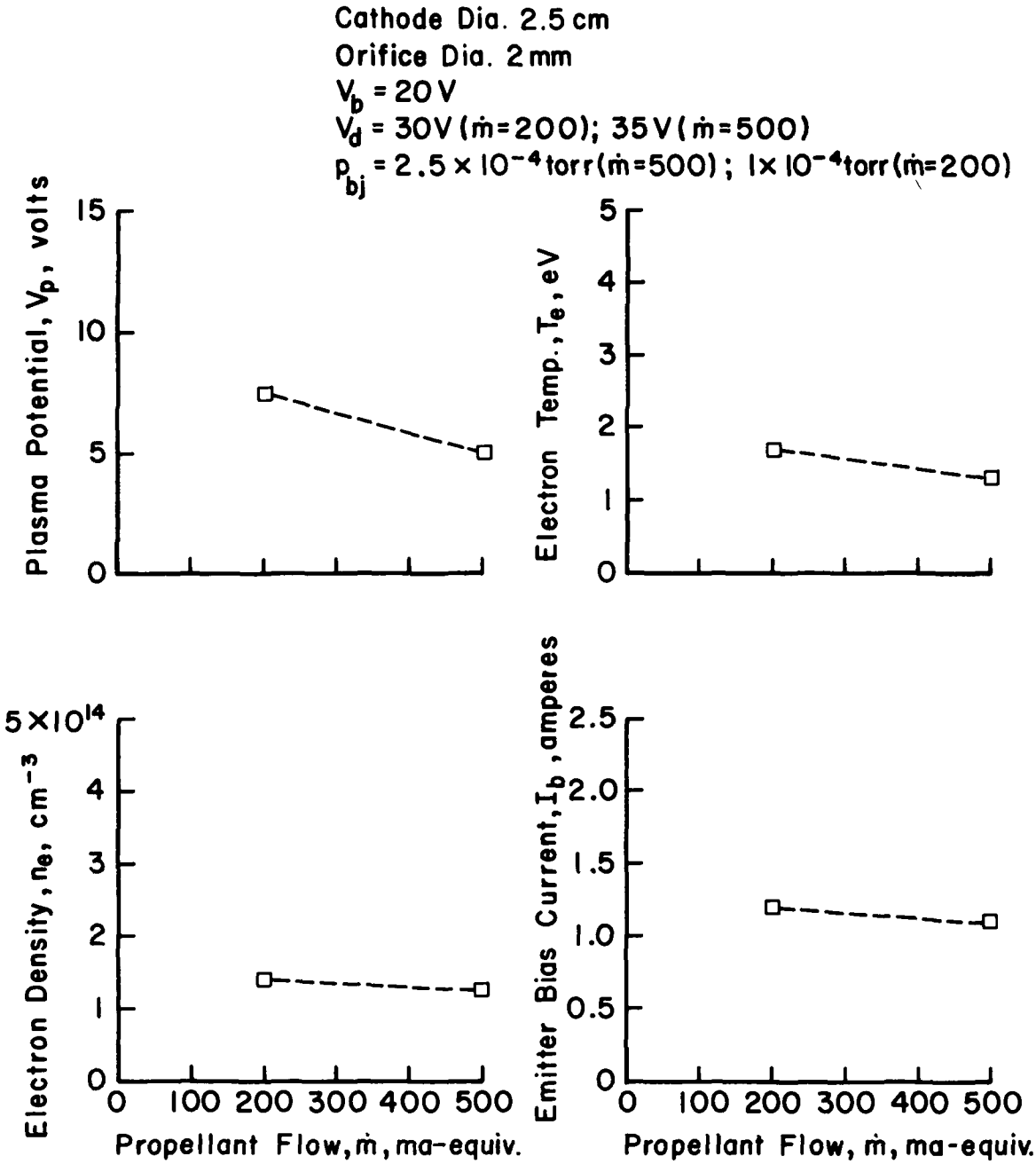

Figure 24. Plasma properties as a function of flow rate.

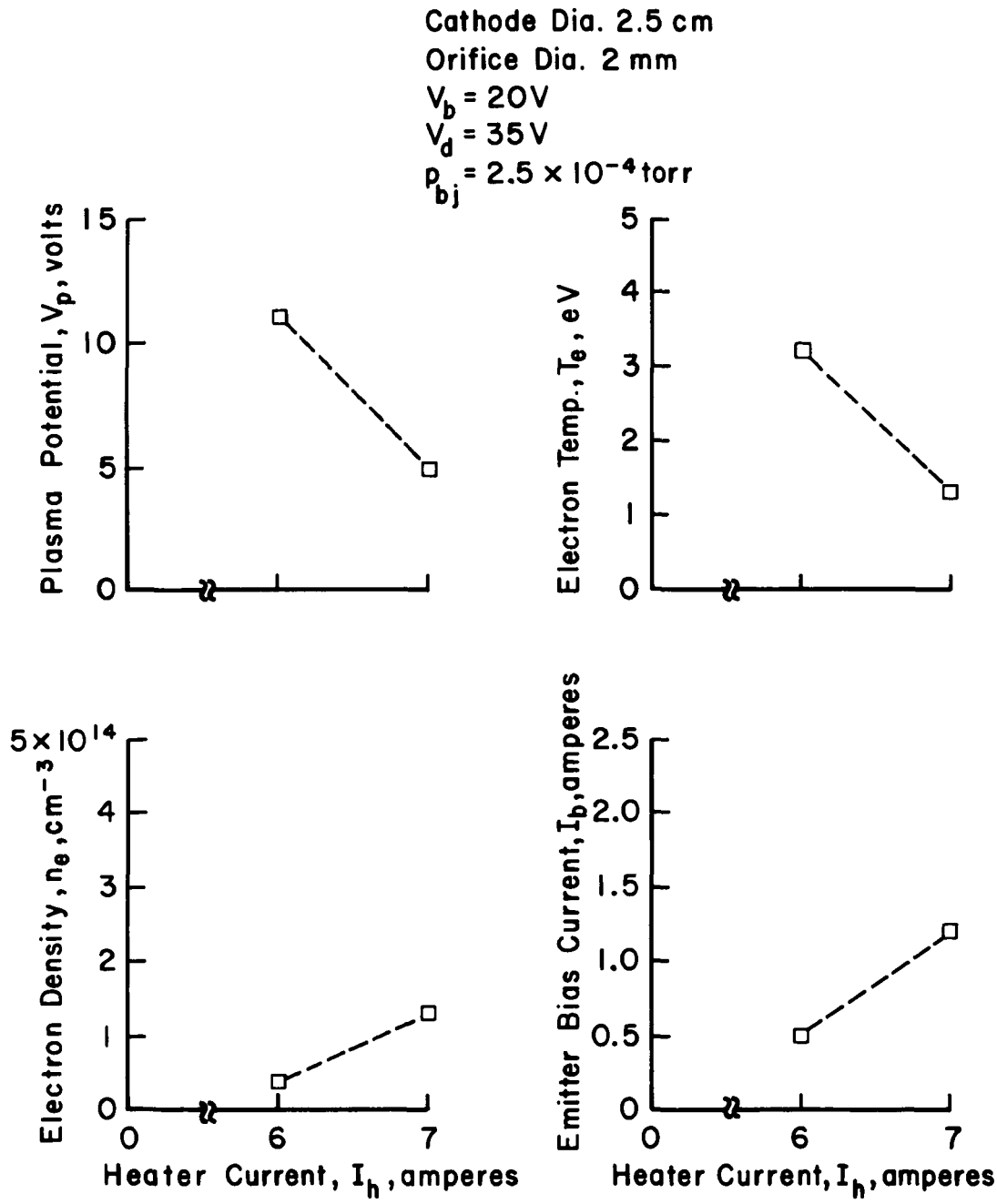

Figure 25. Plasma properties as a function of heater current.

Fig. 26(b), the plasma potential can still be determined, but with less certainty. When the bias voltage is reduced to zero, the plasma potential is no longer evident -- Fig. 26(a). Most probe traces at zero bias were further from the ideal than the one shown in Fig. 26(a), with probe current continuing to increase at an increasing rate as probe potential is raised, until a damaging arc is established.

A possible explanation for the degradation of probe traces at low bias voltage is the presence of high frequency plasma fluctuations. The recording equipment used would average the potential and density fluctuations in the plasma, so that the trace obtained would be a composite of a wide range of instantaneous traces.

The cathode bias circuit was connected to an oscilloscope to look for plasma fluctuations. For the zero bias case of Fig. 26(a), signals of 0.1-7.0 V peak-to-peak were found at about 4×10^5 Hz. At a 10 V bias this signal still appeared to be present, but much weaker. At a 20 V bias, no rapid fluctuation was evident.

Population-potential oscillations are often found in plasmas.[20] The attrition of electrons and ions, with electrons leaving faster because of their low mass, results in the increase in plasma potential. At some value of plasma potential there is a sudden influx of electrons, which produce a new generation of ions due to collisions with background neutrals. Some oscillation of this type appears possible at low bias voltages. The loss of ions would be expected to be related to ion transit time (ion acoustic wave velocity), which is in approximate agreement with the observed frequency. Similar oscillations in discharge current were observed by Byers in mercury hollow cathode tests.[20] Byers found that changes in keeper supply impedance affected both the

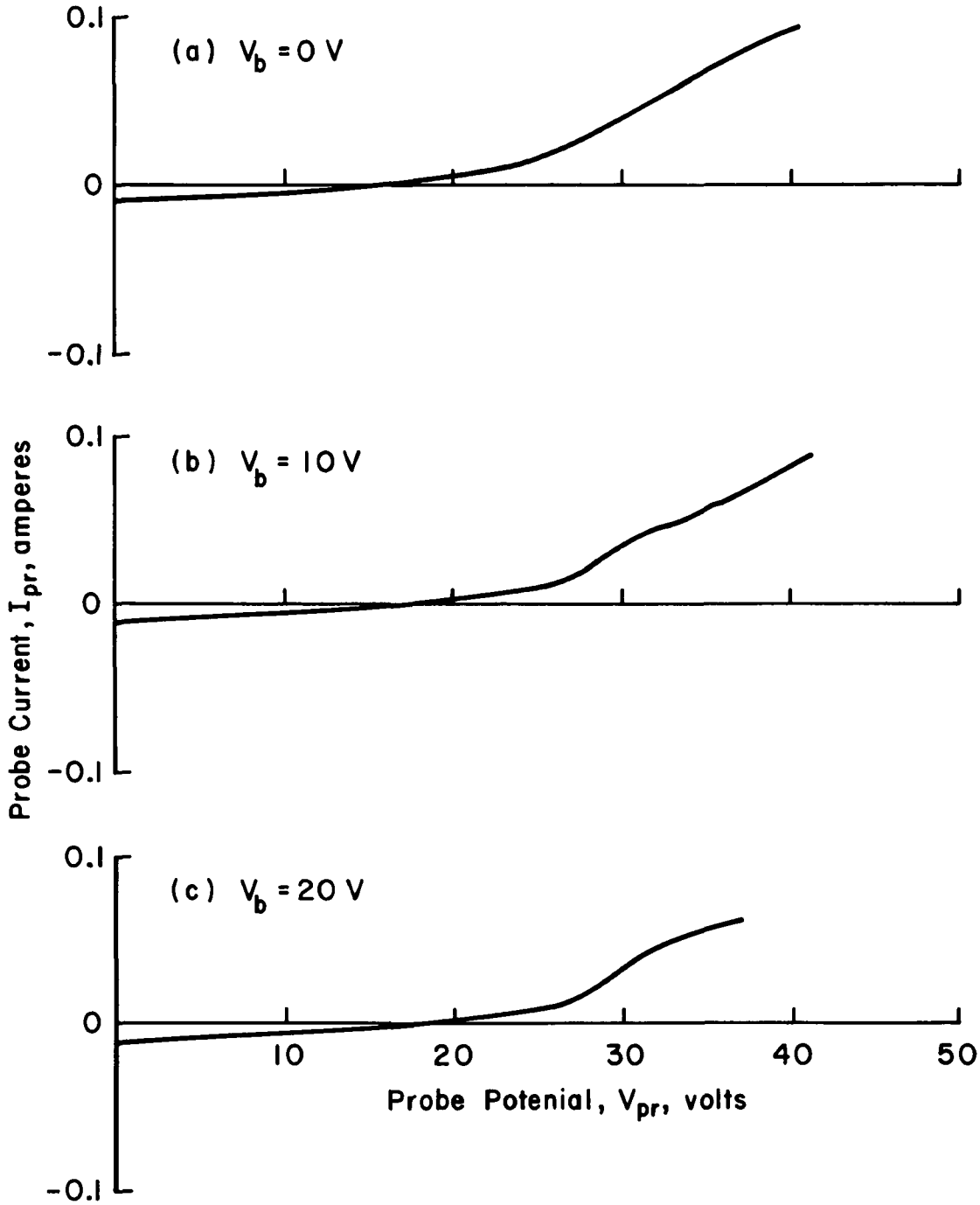

Figure 26. Langmuir probe traces at several different bias voltages.

oscillations and the cathode performance. No changes in power supply impedance were made for the tests reported herein.

Cathode Starting

Ease and reliability of starting were also of interest in this investigation. Normal startup procedure was to obtain an internal cathode chamber discharge by biasing the emitter at -30 V relative to the chamber wall - or internal anode in the case of the discharge chamber cathode. This internal discharge always started if the emitter heater was used (at 6 to 7 amperes) to preheat the cathode chamber for 5 to 10 minutes. Omission of this preheat step sometimes led to erratic startups. The bias current at 30 V was typically 1 to 2 amperes for a heater current of ~ 7 amperes. At this point, initiation of a discharge to the main anode could usually be accomplished by applying normal voltage to the main anode. For low propellant flow rates and/or small orifice diameters (less than 1 mm), a high voltage tickler (about 17 kV maximum) was required to initiate the main discharge. Restarts were easier than the initial startup after pumpdown, probably because contaminants were removed by normal operation.

In summary, the use of an internal emitter and a preheat phase gave 100 percent starting reliability for the internal discharge. Initiation of the discharge to the main anode was more dependent on propellant flow rate and orifice diameter, with increases in both parameters favoring startup of the main discharge.

VI. CONCLUDING REMARKS

Significant progress was made towards longer life argon hollow cathodes. The optimum cathode chamber size was found to be larger than those sizes presently used for mercury hollow cathodes, with optimum diameter in the range from 1.0 to 2.5 cm. This large size permits the use of replaceable internal emitters, as well as the use of more complex internal electrodes. Optimum orifice diameter was also determined. This diameter was found to range from about 0.5 to 5 mm depending on operating conditions. The use of an emitter bias voltage tended to extend the operating range and eliminate internal plasma fluctuations. With a bias voltage of 10 V, operating conditions were found that were favorable for longer orifice lifetimes. Whether or not these lifetimes will be sufficient for electric propulsion applications is not yet clear. An internal emitter was also found to be consistent with reliable starting.

REFERENCES

1. Rawlin, V. K. and W. R. Kerslake, "Durability of the Sert II Hollow Cathode and Future Applications of Hollow Cathodes," AIAA Paper No. 69-304, Williamsburg, Virginia, 1969.

2. Reader, P. D., "The Operation of an Electron-Bombardment Ion Source with Various Gases," NASA TM X-52006, 1964.

3. Byers, D. C. and P. D. Reader, "Operation of an Electron-Bombardment Ion Source Using Various Gases," NASA TN D-6620, 1971.

4. Martin, A. R., "Design and Operation of an Ion Engine Using the Rare Gases," Journal of the British Interplanetary Society, Vol. 26, pp. 742-752, 1973.

5. Martin, A. R., "Ion Production in Argon Ion Engine Discharges," Physica, Vol. 58, pp. 77-87, 1972.

6. Isaacson, G. C. and H. R. Kaufman, "15 CM Multipole Gas Ion Thruster," AIAA Paper No. 76-1045, 1976.

7. Kaufman, H. R., "Technology of Electron-Bombardment Ion Thrusters," Advances in Electronics and Electron Physics, Vol. 36, 1974.

8. Wintucky, E. G., "A 20,000-Hour Endurance Test of a Structurally and Thermally Integrated 5-cm Diameter Ion Thruster Main Cathode," AIAA Paper 75-368, Cleveland, Ohio, 1975.

9. Hudson, W. R. and A. J. Weigand, "Hollow Cathodes with BaO Impregnated, Porous Tungsten Inserts and Tips," AIAA Paper No. 73-1142, Lake Tahoe, Nevada, 1973.

10. Zuccaro, D., "Mercury Vapor Hollow Cathode Component Studies," AIAA Paper No. 73-1141, Lake Tahoe, Nevada, 1973.

11. Milder, N. L. and W. R. Kerslake, "Evaluation of Filament deterioration in Electron-Bombardment Ion Sources," NASA TN D-2173, 1964.

12. Reader, P. D., Private Communication, 1976.

13. Anderson, G. S., "Hg Adsorption Studies Using Atom Ejection Patterns," Journal of Applied Physics, Vol. 36, No. 5, May, 1965

14. Philip, C. M., "The Design and Operation of a Hollow Cathode for Electron Bombardment Ion Thrusters," Royal Aircraft Establishment, TR 69213, 1969.

15. Newsome, D. S., "Significant Structure Theory of Multilayer Physical Adsorption," The Journal of Physical Chemistry, Vol. 78, No. 25, pp. 2600-2604, 1974.

16. Jahn, R. G., Physics of Ion Propulsion, Gordon and Breach, New York, 1966.

17. Fearn, D. G., IEE Conference on Electric Propulsion of Space Vehicles, p. 146, April, 1973.

18. Byers, D. C., "Effect of Power Supply Impedance on the Sert II Neutralizer," NASA TM X-52543, 1969.

19. Strickfaden, W. B. and K. L. Geiler, "Probe Measurements of the Discharge in an Operating Electron Bombardment Engine," AIAA Journal, Vol. 1, No. 8, pp. 1815-1823, 1963.

20. Heer, C. V., Statistical Mechanics, Kinetic Theory, and Stochastic Processes, Academic Press, New York, 1972.

21. Clausing, P., Ann. Phys. (Leipzig), Vol. 12, pp. 961-989, 1932.

APPENDIX

Determination of Pressures Inside the Cathode and Discharge Chamber

Free molecular flow can be assumed for the pressures normally found in the bell jar environment. Consider the escape of a particle with speed v_i from the volume V through an orifice of area dA.[20] (See Fig. 27(a).) For this particle to escape in the time dt and in the direction $d\Omega$, it must lie within the volume element ΔV. The total number of such particles can be calculated as follows:

$$\left\{\begin{array}{l}\text{number of particles}\\ \text{escaping V in time}\\ \text{dt in direction } d\Omega\end{array}\right\} = \sum_i \left(\frac{1}{V}\right) N_i \, v_i \cos\theta dA dt \left(\frac{d\Omega}{4\pi}\right) \qquad (A1)$$

where

$$d\Omega = \sin\theta d\theta d\phi.$$

The average speed, $\bar{v}$, and the average particle density, n, are defined as

$$\bar{v} = \sum_i \frac{N_i v_i}{N} \quad \text{and} \quad n = \frac{N}{V} \qquad (A2)$$

---

20 This pressure determination intially follows the approach of C. V. Heer, Statistical Mechanics, Kinetic Theory, and Stochastic Processes, pp. 10-11.

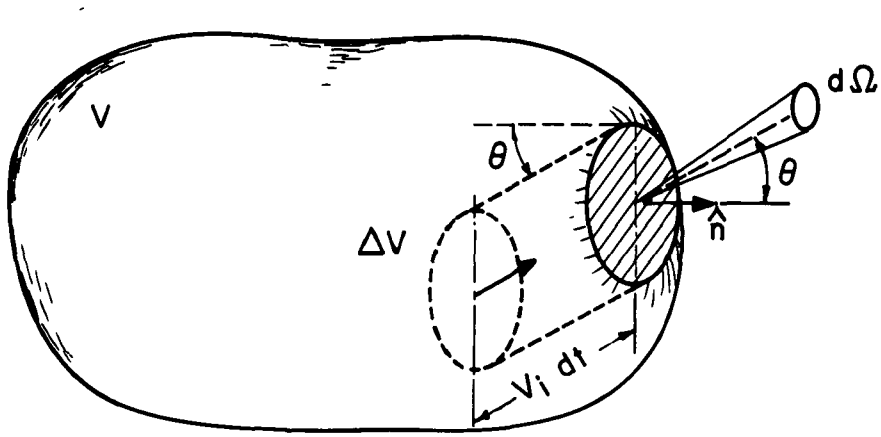

(a)

(a) Escape from volume.

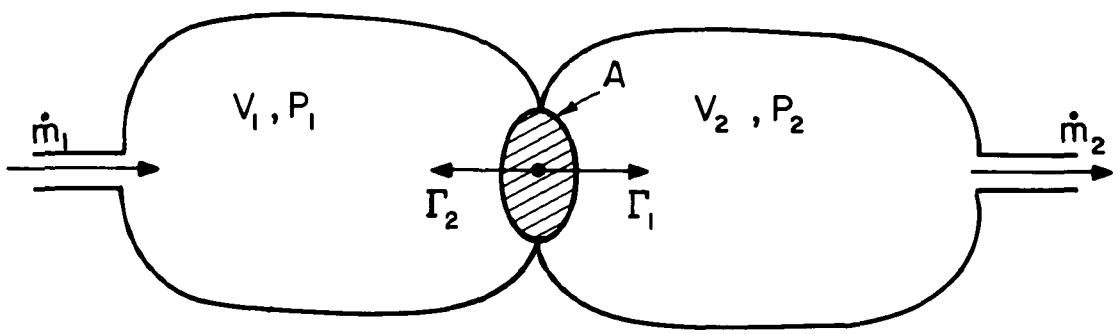

(b)

(b) Flow between two volumes.

Figure 27. Assumed configurations for free molecular flow calculations.

where

N ≡ the total number of particles in volume V. Substituting these expressions into Eq. (A1) results in

$$\left\{\begin{array}{l}\text{number of particles}\\ \text{escaping V in time}\\ \text{dt in direction d}\Omega\end{array}\right\} = n\,\bar{v}\,\cos\theta dA\,dt\,\left(\frac{d\Omega}{4\pi}\right) \tag{A3}$$

Using a unit area for dA and unit time for dt, then the total particle escape rate, Γ (particles/m^2-sec), can be found by integrating over $0 \leq \theta \leq \pi/2$ and $0 \leq \phi \leq 2\pi$, i.e.

$$\Gamma = \frac{1}{4\pi}\int_0^{2\pi} d\phi \int_0^{\pi/2} n\,\bar{v}\,\cos\theta\sin\theta\,d\theta = \frac{1}{4}\,n\,\bar{v} \tag{A4}$$

For an ideal gas, substituting from the expression above gives

$$P = n\,k\,T = \frac{4\Gamma kT}{\bar{v}} \tag{A5}$$

where k is Boltzmann's constant.

In a thruster operating at a steady flow a constant pressure and/or particle density exists within the cathode chamber, the discharge chamber, and the surrounding bell jar region. Since the propellant flow rate is generally known then Γ can be calculated by knowing the open area which separates the two volumes (Fig. 27(b)). In general, the pressures of each volume will be different. For this steady state condition, $\dot{m}_1 = \dot{m}_2 = \dot{m}$ (where $\dot{m}$ is the particle flow rate, typically in ampere-equivalents), and the difference, $\Gamma_1 - \Gamma_2$ is simply

$$\Gamma_{net} = \Gamma_1 - \Gamma_2 = \frac{\dot{m}}{eA} \tag{A6}$$

for $\dot{m}$ in ampere-equivalent, A in m^2, and e is the electronic charge in coulombs. By substituting from Eqs. (A5) and (A6), the pressure difference across the orifice can be found.

$$P_1 - P_2 = \frac{4kT}{\bar{v}} (\Gamma_1 - \Gamma_2) = \frac{4\dot{m}kT}{\bar{v}eA} \quad (\frac{N}{m^2}) \tag{A7}$$

For a Maxwellian energy distribution

$$\bar{v} = \frac{8kT}{\pi m} \tag{A8}$$

and the pressure difference becomes

$$P_1 - P_2 = \frac{\dot{m}}{eA} \sqrt{2\, mkT} \quad (\frac{N}{m^2}) \tag{A9}$$

Using Eq. (A9) the pressure in the cathode chamber, P_c, can be found. (Actually, the densities found within the hollow cathode chamber are in a transition regime between free molecular and continuum flow exists. However, results using this calculation appear to be in good agreement with experiment.) For example, let $\dot{m}$ = 0.5 amp-equiv., A = $7.9 \times 10^{-7} m^2$ (a 1 mm orifice), and T = 500°K. The discharge chamber pressure, P_d, will later be shown to be much less than P_c, so that the return flow is negligible. From Eq. (A9), then

$$P_c = 214 \text{ N/m}^2 = 1.6 \text{ torr.} \quad (\text{for } P_c >> P_d)$$

Similarly, P_d can be found if the bell jar pressure, P_{bj}, is known. Using the same values for $\dot{m}$ and T, and letting $P_{bj} = 2 \times 10^{-4}$ torr with A = 88 cm^2 (open area for the screen grid used), then

$$P_d = 3.4 \times 10^{-4} \text{ torr} = 1.7\, P_{bj} \quad \text{Note that } P_d << P_c.$$

If the finite thickness of the screen grid is considered then the effective open area is reduced by the clausing factor[21] which is determined by the hole thickness to diameter ratio. For the screen grid used, the clausing factor, K_c, was 0.81. P_d is therefore increased by the factor $1/K_c$. That is

$$P_d = \left(\frac{1}{0.81}\right) (3.4\text{x}10^{-4}\text{torr}) = 4.2\text{x}10^{-4}\text{torr} = 2.1\ P_{bj}$$

when the clausing factor is included.

DISTRIBUTION LIST

	No. of Copies
National Aeronautics and Space Administration Washington, D. C. 20546	
Attn: RPE/Mr. Wayne Hudson	1
Mr. Daniel H. Herman, Code SL	1
National Aeronautics and Space Administration Lewis Research Center 21000 Brookpark Road Cleveland, Ohio 44135	
Attn: Research Support Procurement Section	
Mr. Allen Jones, MS 500-313	1
Technology Utilization Office, MS 3-19	1
Report Control Office, MS 5-5	1
Library, MS 60-3	2
N. T. Musial, MS 500-113	1
Spacecraft Technology Division, MS 54-1	
Mr. E. Davison	1
Mr. R. Finke	1
Mr. D. Byers	1
Mr. B. Banks	1
Mr. S. Domitz	1
Mr. F. Terdan	1
Mr. P. Thollot	1
Mr. W. Kerslake	1
Mr. E. Theman	1
Mr. M. Mirtich	10
Physical Science Division, MS 301-1	
Mr. W. E. Moeckel	1
National Aeronautics and Space Administration Marshall Space Flight Center Huntsville, Alabama 35812	
Attn: Mr. Jerry P. Hethcoate	1
Research and Technology Division Wright-Patterson AFB, Ohio 45433	
Attn: (ADTN) Lt. David A. Fromme	1
NASA Scientific and Technical Information Facility P. O. Box 8757 Baltimore/Washington International Airport Baltimore, Maryland 21240	40
Case Western Reserve University 10900 Euclid Avenue Cleveland, Ohio 44106	
Attn: Dr. Eli Reshotko	1

Royal Aircraft Establishment
Space Department
Farnborough, Hants, England
Attn: Dr. D. G. Fearn 1

United Kingdom Atomic Energy Authority
Culham Laboratory
Abingdom, Berkshire, England
Attn: Dr. P. J. Harbour 1
Dr. M. F. A. Harrison 1
Dr. T. S. Green 1

National Aeronautics and Space Administration
Goddard Space Flight Center
Greenbelt, Maryland 20771
Attn: Mr. W. Isley, Code 734 1
Mr. R. Hunter 1
Mr. R. Callens, Code 734 1

SAMSO
Air Force Unit Post Office
Los Angeles, California 90045
Attn: Capt. D. Egan/SYAX 1

Comsat Laboratories
P. O. Box 115
Clarksburg, Maryland 20734
Attn: Mr. B. Free 1
Mr. O. Revesz 1

Rocket Propulsion Laboratory
Edwards AFB, California 93523
Attn: LKDA/Mr. Frank Mead 2

DFVLR - Institut für Plasmadynamik
Technische Universitat Stuttgart
7 Stuttgart-Vaihingen
Allmandstr 124
West Germany
Attn: Dr. G. Krülle 1

DFVLR - Institut für Plasmadynamik
33 Braunschweig
Bienroder Weg 53
West Germany
Attn; Mr. H. Bessling 1

Giessen University
1st Institute of Physics
Giessen, West Germany
Attn: Professor H. W. Loeb 1

Jet Propulsion Laboratory
4800 Oak Grove Drive
Pasadena, California 91102
Attn: Dr. Kenneth Atkins 1
Technical Library 1
Mr. Eugene Pawlik 1
Mr. James Graf 1
Dr. John R. Beattie 1

Electro-Optical Systems, Inc.
300 North Halstead
Pasadena, California 91107
Attn: Mr. R. Worlock 1
Mr. E. James 1

TRW, Inc.
TRW Systems
One Space Park
Redondo Beach, California 90278
Attn: Mr. M. Huberman 1
Dr. J. M. Sellen 1

National Aeronautics and Space Administration
Ames Research Center
Moffett Field, California 94035
Attn: Technical Library 1

National Aeronautics and Space Administration
Langley Research Center
Langley Field Station
Hampton, Virginia 23365
Attn: Technical Library 1

Hughes Research Laboratories
3011 Malibu Canyon Road
Malibu, California 90265
Attn: Dr. Jay Hyman 1
Mr. J. H. Molitor 1
Mr. T. D. Masek 1
Dr. R. L. Poeschel 1
Mr. R. Vahrenkamp 1

United States Air Force
Office of Scientific Research
Washington, D. C. 20025
Attn: Mr. M. Slawsky 1

Princeton University
Princeton, New Jersey 08540
Attn: Mr. W. F. Von Jaskowsky 1
Dean R. G. Jahn 1
Dr. K. E. Clark 1

Communications Research Centre
Ottawa, Ontario, Canada
Attn: Dr. W. F. Payne 1

Joint Institute for Laboratory Astrophysics
University of Colorado
Boulder, Colorado 80302
Attn: Dr. Gordon H. Dunn 1

Department of Aeronautics and Astronautics
Stanford University
Stanford, California 94305
Attn: Professor Howard S. Seifert 1

Boeing Aerospace Co.
P. O. Box 3999
Seattle, Washington 98124
Attn: Mr. Donald Grim 1

Intelcom Rad Tech
7650 Convoy Court
P. O. Box 80817
San Diego, California 92138
Attn: Dr. David Vroom 1

Lockheed Missiles and Space Company
Sunnyvale, California 94088
Attn: Dr. William L. Owens
Propulsion Systems, Dept. 62-13 1

Fairchild Republic Company
Farmingdale, New York 11735
Attn: Dr. William Guman 1

COMSAT Corporation
950 L'Enfant Plaza SW
Washington, D. C. 20024
Attn: Mr. Sidney O. Metzger 1

Electrotechnical Laboratory
Tahashi Branch
5-4-1 Mukodai-Machi, Tanashi-Shi
Tokyo, Japan
Attn: Dr. Katsuva Nakayama 1

Office of Assistant for Study Support
Kirtland Air Force Base
Albuquerque, New Mexico 87117
Attn: Dr. Calvin W. Thomas OAS Ge 1
Dr. Berhart Eber OAS Ge 1

Bell Laboratories
600 Mountain Avenue
Murray Hill, New Jersey 07974
Attn: Dr. Edward G. Spencer 1
Dr. Paul H. Schmidt 1

Massachusetts Institute of Technology
Lincoln Laboratory
P. O. Box 73
Lexington, Massachusetts 02173
Attn: Dr. H. I. Smith 1

December 16, 1976

TO: NASA Distribution List

RE: Correction to NASA CR-135102 under Grant NSG-3011

After publication a correction was found concerning NASA CR-135102 under Grant NSG-3011. Reported electron densities in the hollow cathode chamber were 100 times too high. On page 41 the last sentence should read: "The electron density is ~$10^{12}/cm^3$ (below a 35 V discharge), which is ~10 times more dense than a typical ion thruster discharge chamber." In Figs. 23-24 the electron density exponent should be 12 not 14.